Effect of flexibility on the self-propelled locomotion by an elastically supported stiff foil actuated by a torque

P. E. Lopez-Tello📷 and R. Fernandez-Feria📷*
Fluid Mechanics Group, University of Malaga, Dr Ortiz Ramos s/n, 29071 Malaga, Spain

A theoretical model is presented for the locomotion of an aquatic vehicle propelled by a flexible foil elastically mounted to translational and torsional springs and dampers at an arbitrary pivot axis and actuated by a harmonic torque. The work extends a previous model by the authors for an elastically mounted rigid foil [Lopez-Tello *et al.*, Appl. Math. Model. **116**, 236 (2023)], allowing for a passive flexural motion of the foil in addition to the passive pitching and heaving motions of the rigid foil, all of them generated by the actuating torque and the fluid-foil interaction. The Euler-Bernoulli beam equation is used together with linearized results from the potential flow theory, valid for small pitch, heave, and flexural deflection amplitudes. The problem is governed by four ordinary differential equations (ODEs) for the temporal evolutions of the swimming velocity, and the pitch, heave, and flexural motions of the flexible foil. In addition to numerical results of these ODEs, we also present an analytical perturbation solution, which provides a valuable quick insight about the propulsion performance, but which is additionally restricted to very small swimming velocities. The vehicle's propulsion performance is discussed in terms of the foil stiffness ratio and the remaining nondimensional parameters, particularly the translational and torsional spring constants, the pivot axis location, and the Lighthill number. It is found that, except for very low Lighthill numbers, the maximum swimming velocity is reached for a rigid foil actuated at the leading edge with the resonant combination of the translational and torsional springs constants for the given frequency. However, higher propulsive efficiencies and lower costs of transport, but with slightly smaller swimming velocities, are obtained for flexible foils with the same resonant combination of the elastic supports at the leading edge. As a validation of the model, the Strouhal number for optimal propulsion efficiency is found in a narrow band around 0.32, in agreement with many experimental and numerical works on optimal propulsion by flapping foils. Additionally, the relation between Strouhal and Lighthill numbers for optimal propulsion is favorably compared with experimental data for fishes where the primary mechanism for producing thrust is an oscillatory prominent caudal fin.

I. INTRODUCTION

Motivated by the highly efficient propulsion of fishes that produce most of their thrust by the oscillatory motion of their caudal fins, an increasing number of works have been dedicated in the recent past to the study of flapping foils to propel bioinspired aquatic vehicles [1–9]. Many works have analyzed the effect of chordwise flexibility of the foil, which in general has been shown to enhance the propulsion performance in terms of thrust, efficiency, and cruising velocity [10–19], as well as the efficiency of the closely related flapping-foil energy harvesters [20–27].

---

*ramon.fernandez@uma.es

Particularly helpful for the understanding of the propulsive performance of swimming animals, and for the design and improvement of bioinspired swimming robotic models, is to dispose of analytical solutions characterizing the fluid-structure interaction of flexible flapping foils, even for very simplified configurations. These analytical approximations have to be searched within the framework of the two-dimensional and linearized inviscid flow theory for small deformations of the foil, pioneered by Wu [28], who considered a flapping plate that incorporated flexibility, allowing it to deform according to the fluid and elastic forces it experiences. Passive flexibility changes the thrust that a flapping plate generates, and consequently its propulsive efficiency and its cruising speed if self-propelled. It has generally been found from these inviscid flow theories that flexibility produces greater thrust when actuated near a fluid-structure natural frequency, but less otherwise, with larger propulsive efficiency than that of a rigid foil over a broad range of stiffnesses and frequencies [29–36]. However, when viscous flow with nonlinearities associated to flow separation are considered, optimal performance can be achieved off the structural resonance conditions [37–43]. In any case, structural resonance plays always a relevant role in enhancing the propulsion performance if the mass ratio of the foil is not too large [44], as it is the case in fishlike swimming.

In the present work we consider the locomotion of an aquatic vehicle propelled by an elastically mounted foil actuated by an oscillatory torque and analyze the effect of chordwise flexibility on the propulsion performance. Due to the driving torque applied on a given pivot axis, at which the foil is attached to longitudinal and torsional springs and dampers, the foil undergoes passive pitching, heaving, and flexural deflection motions. We use a model for the fluid-foil interaction based on the Euler-Bernoulli beam equation coupled to the results from linear potential flow theory [36], valid for small pitching, heaving, and flexural deflection amplitudes, and therefore for sufficiently high stiffness of the foil, together with a constant drag coefficient for the vehicle of a given mass. In a recent work we have considered this model for the case of the vehicle propelled by a rigid foil elastically supported [45], finding that the optimal propulsive performance, i.e., maximum cruising velocity and maximum propulsive efficiency, is reached for particular resonant combinations of the torsional and longitudinal springs constants for an oscillatory torque with a given frequency actuating at, or close to, the foil's leading edge. It was shown that the propulsion enhancement due to this resonant behavior, which was approximately characterized by simple analytical expressions, is quite significant, diminishing more than twice both the swimming velocity and the propulsive efficiency by just moving the torsional spring constant a few percent from its resonant value. The model for the rigid-foil flapper was validated with high Reynolds numerical simulations of a self-propelled pitching foil, and by the fact that the Strouhal number for optimal propulsion was in agreement with that found experimentally in nature for optimal cruise propelled by flapping fins or wings. When chordwise flexibility of the foil is taken into account, the model is substantially more complicated because so it is the fluid-structure interaction of the propeller. However, using the analytical results of Refs. [36,46] for this interaction, assuming a quartic polynomial for the flexural deflection of the foil, the resulting model is governed by four ordinary differential equations, just one more equation than for the rigid-foil counterpart. In addition to the results from the numerical integration of these equations, which is straightforward and almost instantaneous compared with numerical computations of the full viscous problem, we also derive simple analytical expression in the limit of very small nondimensional swimming velocity, which, contrary to the flapping amplitudes, is not limited in the numerical solutions of the model equations. The resulting approximate analytical expressions provide simple scaling laws for the nondimensional performance parameters, such as cruising velocity, propulsive efficiency, cost of transport, and Strouhal number, in terms of the nondimensional driving torque amplitude, vehicle's drag, characterized by the Lighthill number, and mass ratio, among others.

The literature on the propulsive performance of flexible flapping foils is vast. Most of the works are for oscillating foils in a fluid stream with fixed velocity rather than for self-propelled flexible foils, a few of them for a vehicle or body propelled by a flexible flapping foil, and none of them, to the best of our knowledge, for the present configuration of a flexible foil elastically mounted on the

vehicle hull through translational and torsional springs and dampers that allows for passive heaving, pitching, and flexural deflection motions. As aforementioned, numerous theoretical, computational, and experimental studies on flexible flapping foils with prescribed pitching and/or heaving motions and passive flexural deflection immersed in a constant velocity stream show that structural resonance may play a relevant role in their propulsive performance, generally enhancing the thrust generation and/or the propulsive efficiency when actuated at, or near, structural resonance frequencies, depending on the prescribed kinematics, the flow regime, and the relative inertia of the foil [29–31,33–36,44,47,48]. Another kind of structural resonance that may enhance the propulsive performance of rigid foils oscillating in a fluid stream with fixed velocity appears when the foil, actuated with forced pitching or heaving motion, is elastically mounted to translational or torsional springs and dampers, so that the heaving or the pitching motion is also passive [49–52]. The new structural resonances, associated to the supporting springs and dampers and with natural frequencies quite different from those associated to the flexural deflection in the case of flexible foils, may enhance the propulsive performance even more than the resonantlike response without springs and dampers [26,27,50,53]. In any case, these flexible foils elastically mounted may be actuated in a greater variety of coupled natural frequencies to improve their propulsive performance.

When the flexible oscillating foil is not immersed in a constant velocity fluid stream but moves freely self-propelled by itself, or propelling an animal or a vehicle, the problem is quite different because the velocity of the foil relative to the flow, i.e., the free-swimming velocity, is no longer an independent control parameter, nor is it constant, but it is time dependent and resulting from the fluid-structure interaction, and therefore a function of the kinematics and structural properties of the foil. Alben *et al.* [32] found resonance peaks in the inviscid free-swimming velocity of an elastic oscillating plate, similar to those found for a flexible foil immersed in a fluid stream with fixed velocity [30]. However, only some general results for a foil in a fixed-velocity stream can be roughly extrapolated, in certain circumstances, to the time-averaged performance of these freely moving foils when using the time-averaged swimming velocity [32,41,54]. For consistent and accurate results one has to solve the complex fluid-structure interaction problem of the freely moving body. Olivier and Dumas [41] considered numerically the self-propelled locomotion at low flapping Reynolds numbers of a flexible plate with imposed pitching and heaving motion about its leading edge and with a drag model, finding that increasing the flexibility decreases the time-averaged swimming velocity. This result is in contradiction with similar low Reynolds number numerical results but with only heaving motion imposed at the leading edge of the foil, where moderate flexibility usually implies a significant increase of the averaged swimming velocity near the first resonant frequency [47,55] or at much lower frequencies [56,57]. In particular, Yeh and Alexeev [47] found that elastic propulsors can be operated at a regime of maximum propulsion near the first resonant frequency, or maximum efficiency when operated away from the resonance. Hoover *et al.* [58] further confirmed these results with three-dimensional simulations, giving additional insight about the role of resonance in swimming performance. More efficient aquatic locomotion (higher cruising speed and efficiency) has been found for an elastic plate actuated at resonance by combined external and internal actuation, with heaving motion at the leading edge and distributed internal bending moment [59], or using an optimal stiffness distribution of the heaving flexible plate [60]. However, neither of these works considered the mass nor the form of the aquatic vehicle propelled by the flexible foil, and therefore the vehicle's inertia and drag as independent parameters that affect to its locomotion. We show in the present work that the relevant structural resonances optimizing the locomotion through elastically mounted flexible foils with high enough stiffness are associated to the stiffness of the supporting springs, which are quite different from the aforementioned flexural resonances. Also, that these spring resonances eclipse the structural resonances associated to the chordwise deflection of the foil, qualitatively in agreement with previous theoretical works for oscillating foils in a fluid stream with fixed velocity [26,27,53]. Unfortunately, to the best of our knowledge, no numerical nor experimental results on the locomotion through elastically mounted flexible foils are available to compare with.
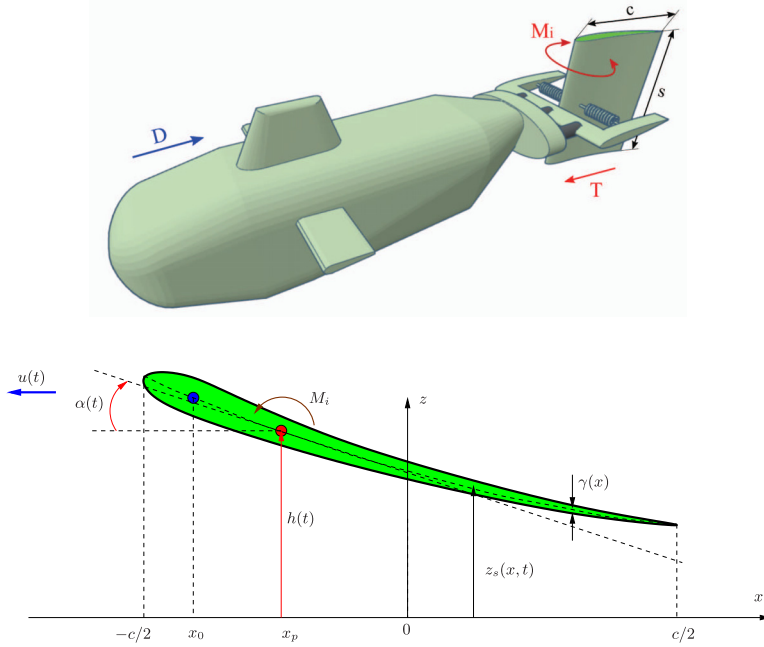
FIG. 1. Schematic of an underwater vehicle (top) propelled by a flexible foil (bottom).

II. FORMULATION OF THE PROBLEM

We consider an aquatic vehicle self-propelled by a flexible hydrofoil [see sketch in Fig. 1 (top)] of chord length c and large aspect ratio s/c, where s is the foil span, so that the flow around it may be considered two dimensional in the plane (x, z) shown in the bottom of Fig. 1. The foil is elastically mounted to translational and torsional springs and dampers at a given pivot axis x_p, and actuated at the same pivot with a known torque M_i, per unit span, to generate the pitching motion that, together with the induced passive heaving and flexural deflection motions of the foil, propels the vehicle. In particular, a harmonic torque with frequency ω,

$$M_i = A_M \sin(\omega t), \tag{1}$$

will be assumed, with the amplitude A_M sufficiently small for the amplitudes of all the foil's motions be small compared to c. Thus, one may use Euler-Bernoulli's beam equation to describe the motion of the foil centerline $z_s(x, t)$ [36]:

$$\rho_s \gamma \frac{\partial^2 z_s}{\partial t^2} + \frac{\partial^2}{\partial x^2} \left(\frac{E \gamma^3}{12} \frac{\partial^2 z_s}{\partial x^2} \right) + L_o \delta(x - x_p) - M_o \delta'(x - x_p) = \Delta p - M_i \delta'(x - x_p), \tag{2}$$

for $-c/2 \leqslant x \leqslant x/2$. In this equation ρ_s, γ, and E are the density, thickness, and elastic modulus of the foil, respectively,

$$L_o = k_h h + b_h \frac{dh}{dt} \qquad \text{and} \qquad M_o = -k_\alpha \alpha - b_\alpha \frac{d\alpha}{dt} \tag{3}$$

are the force and moment per unit span exerted by the foil on the translational and torsional springs and dampers at the pivot axis, where $h(t)$ and $\alpha(t)$ characterize its heaving and pitching motions, respectively, and k_h, k_α, b_h, and b_α are the respective constants of the springs and dampers. Note that α is taken positive clockwise following the usual convention in aerodynamics, while the moments M_o and M_i are positive counterclockwise. Finally, $\Delta p = p^- - p^+$ is the pressure difference between the lower and upper sides of the foil, which is the only force (per unit area) that the fluid exerts on

the foil considered in the present inviscid model, valid for sufficiently high Reynolds numbers. Actually, we will use the results from linear potential flow theory for the pressure and, therefore, for the resulting fluid force and moment, because of the aforementioned additional assumption of small-amplitude foil motion (see below for more details). Thus, following Ref. [36], a quartic approximation is used for z_s,

$$z_s(x, t) = h(t) - (x - x_p)\alpha(t) + (x - x_p)^2 d(t) - (x - x_p)^3 \frac{2d(t)}{3(c/2 - x_p)} + (x - x_p)^4 \frac{d(t)}{6(c/2 - x_p)^2},$$
(4)

which accounts for the (passive) heaving and pitching motions, $h(t)$ and $\alpha(t)$, respectively, at $x = x_p$, and for a free trailing edge, $\partial^2 z_s / \partial x^2 = \partial^3 z_s / \partial x^3 = 0$ at $x = c/2$.

The other fundamental equation of the model is Newton's equation in the x direction applied to the vehicle center of mass,

$$m' \frac{du}{dt} = sT - D,$$
(5)

where m' is the vehicle's mass, u the velocity component of its center of mass in the $-x$ direction, D the drag force exerted by the fluid on the whole vehicle, which will be modeled below through a constant drag coefficient, and T the thrust force (per unit span s) generated by the oscillating foil through its interaction with the fluid. This force will also be modeled below using the results from linear, two-dimensional potential flow theory.

A. Nondimensional formulation

Dimensionless variables and parameters will be used from this point on using ω^{-1} and $c/2$ as the time and length scales, respectively, and the fluid density ρ to scale mass units. The same letters will be used for the dimensionless variables, except otherwise specified. For instance, $\omega t \to t$ is now the dimensionless time, $2x/c \to x$ the dimensionless x coordinate, and similarly z, $2u/(c\omega) \to u$, the dimensionless x component of the vehicle's velocity, etc. Note that this velocity thus scaled is actually the inverse of the reduced frequency k commonly used in unsteady aerodynamics [61], which now depends on time,

$$k(t) \equiv \frac{1}{u(t)},$$
(6)

This unsteady reduced frequency will be used in the models for the dimensionless force and moment. All variables and parameters used from this point downward are dimensionless, unless explicitly specified that it is a dimensional quantity, or marked by a tilde (˜) to differentiate it from its dimensionless counterpart. Nonetheless, sometimes a variable is specified as dimensionless just to remark it.

Starting with Eq. (5), its dimensionless counterpart can be written as

$$R'\dot{u} = \hat{C}_T - \text{Li}u^2,$$
(7)

where a dot denotes a derivative with respect to the (now dimensionless) time t,

$$R' = \frac{4m'}{\pi \rho c^2 s}, \quad \text{Li} = \frac{A_w}{\pi c s} C_D, \quad C_D = \frac{2D}{\rho A_w \tilde{u}^2},$$
(8)

are the dimensionless vehicle's mass and Lighthill's number based on a constant drag coefficient C_D, respectively, with A_w a characteristic surface for the vehicle's drag (all quantities in the right-hand sides of these three expressions are dimensional except for C_D and the pure numbers). The thrust

coefficient of the hydrofoil,

$$\hat{C}_T = \frac{8T}{\pi \rho c^3 \omega^2} = \frac{u^2 C_T}{\pi} = \frac{C_T}{\pi k^2}, \tag{9}$$

is written with a hat ($\hat{\ }$) to remark that it is not the standard thrust coefficient C_T scaled with $\rho c \tilde{u}^2/2$, also included in the above relations for reference sake. The expression of $\hat{C}_T$ obtained from linear potential flow theory for a flexible foil moving according to (4) with harmonic functions $h(t)$, $\alpha(t)$, and $d(t)$ was obtained in Ref. [46] and reproduced in Appendix A.

Since $\hat{C}_T(t)$ depends on $h(t)$, $\alpha(t)$, and $d(t)$, to solve Eq. (7) for $u(t)$ one needs additional equations for these functions of time. The first of these equations is obtained by integrating (2) along the foil's chord length, once (4) is substituted, and the remaining two equations by multiplying (2) by $(\tilde{x} - \tilde{x}_p)$ and by $(\tilde{x} - \tilde{x}_p)^2$ and again integrating along the chord length. Assuming that the (dimensional) stiffness $E\gamma^3$ does not depend on $\tilde{x}$, in dimensionless form these equations can be written as [36]

$$R[\ddot{h} + (a - x_0)\ddot{\alpha} + J_a\ddot{d}] = \hat{C}_L - \hat{C}_{L_o}, \tag{10}$$

$$R[(x_0 - a)\ddot{h} - I_a\ddot{\alpha} + J_d\ddot{d}] = 2(\hat{C}_M + \hat{C}_{M_i} - \hat{C}_{M_o}), \tag{11}$$

$$R(I_a\ddot{h} - I_d\ddot{\alpha} + K_d\ddot{d}) + \frac{a^2 + \frac{1}{3}}{3(1-a)^2} S d = \hat{C}_F, \tag{12}$$

where the terms corresponding to the pressure force that the fluid exerts on the foil are

$$\hat{C}_L = \frac{8L}{\pi \rho c^3 \omega^2} = \frac{u^2 C_L}{\pi}, \quad \hat{C}_M = \frac{8M}{\pi \rho c^4 \omega^2} = \frac{u^2 C_M}{\pi}, \quad \hat{C}_F = \frac{32F}{\pi \rho c^5 \omega^2} = \frac{u^2 C_F}{\pi}, \tag{13}$$

with the dimensional forces and moments

$$L = \int_{-c/2}^{c/2}(\Delta p)d\tilde{x}, \quad M = \int_{-c/2}^{c/2}(\tilde{x} - \tilde{x}_p)(\Delta p)d\tilde{x}, \quad F = \int_{-c/2}^{c/2}(\tilde{x} - \tilde{x}_p)^2(\Delta p)d\tilde{x}. \tag{14}$$

Again, the relations between the standard force, moment, and flexural coefficients C_L, C_M and C_F and the hatted ones scaled with the frequency ω, more appropriate for the present self-propulsion problem, are also given in Eq. (13). The expressions of these coefficients obtained in Refs. [36,46] from the linear potential flow theory are given in Appendix A. Similarly, the nondimensional coefficients k_h, k_α, b_h, and b_α associated to Eq. (3), corresponding to the translational and torsional springs and dampers, are defined as

$$\hat{C}_{L_o} = \frac{8L_o}{\pi \rho c^3 \omega^2} = k_h h + b_h \dot{h}, \quad \hat{C}_{M_o} = \frac{8M_o}{\pi \rho c^4 \omega^2} = -k_\alpha \alpha - b_\alpha \dot{\alpha}. \tag{15}$$

The nondimensional input torque (1) is

$$\hat{C}_{M_i} = \frac{8M_i}{\pi \rho c^4 \omega^2} = \epsilon \sin t, \quad \epsilon = \frac{8A_M}{\pi \rho c^4 \omega^2}, \tag{16}$$

where ϵ is assumed sufficiently small to generate the small-amplitude foil motion required by the present model; i.e., $|h| \ll 1$, $|\alpha| \ll 1$, and $|d| \ll 1$. The remaining nondimensional parameters in Eqs. (10)–(12) are the mass and stiffness ratios of the foil,

$$R = \frac{4m}{\pi \rho c^2}, \quad S = \frac{64E\gamma^3}{\pi \rho c^5 \omega^2}, \tag{17}$$

respectively, with $m = \int_{-c/2}^{c/2} \rho_s \gamma d\tilde{x}$ the (dimensional) mass of the foil per unit span, $\tilde{x}_0$ the foil's center of mass, defined as $m\tilde{x}_0 = \int_{-c/2}^{c/2} \tilde{x}\rho_s\gamma d\tilde{x}$, $a = 2\tilde{x}_p/c$ is the dimensionless pivot axis location, $a = -1$ corresponding to the leading edge and $a = 1$ to the trailing edge, and the coefficients J_a, I_a,

J_d, I_d, and K_d are functions of a given in Appendix B for the simplest case of constant ρ_s and γ; i.e., when $m = \rho_s c \gamma$ and $\tilde{x}_0 = 0$.

B. Performance parameters

Once Eqs. (7) and (10)–(12) are solved, either numerically (Sec. III A) or analytically for small u (Sec. III B), one is interested in different nondimensional quantities, in addition to the swimming velocity $u(t)$ itself, that provide relevant information about the self-propelled vehicle's performance.

One of them is the efficiency, defined as the propulsion power, $u(t)\hat{C}_T(t)$ in dimensionless form, divided by the power input spent to generate that propulsion, which in dimensionless form is

$$\hat{C}_{P_i}(t) = -2\dot{\alpha}\hat{C}_{M_i}(t) = -2\dot{\alpha}\,\epsilon\,\sin t. \tag{18}$$

Thus, the instantaneous propulsive efficiency is

$$H(t) = \frac{u(t)\hat{C}_T(t)}{\hat{C}_{P_i}(t)}. \tag{19}$$

Since the forcing torque is a periodic function of time, one expects that so will be the long time solutions of Eqs. (7) and (10)–(12), at least approximately. Of particular interest are thus some time-averaged quantities. For any magnitude $\phi(t)$, its time average over n cycles, once the permanent state for $t \gg 1$ has been reached, is denoted by an overline and given by

$$\overline{\phi} = \frac{1}{2\pi n} \int_t^{t+2\pi n} \phi(t)\,dt, \quad t \gg 1. \tag{20}$$

Different values of n will be used in the reported results, $n = 1$ if the solution is exactly periodic (e.g., for the approximate analytical solutions), or large enough for $\overline{\phi}$ to be almost independent of the choice of n. The most relevant time-averaged quantities are the mean swimming speed, $U = \overline{u}$, and the propulsive (Froude) efficiency:

$$\eta = \overline{H} = \frac{\overline{u\hat{C}_T}}{\overline{\hat{C}_{P_i}}} \simeq \frac{\mathrm{Li}\,\overline{u^3}}{\overline{\hat{C}_{P_i}}}, \tag{21}$$

where Eq. (7) has been used in the last expression, taking into account that $\overline{u\dot{u}} \simeq 0$ if a nearly harmonic swimming velocity $u(t)$ has been reached for $t \gg 1$.

Instead of the swimming velocity U sometimes is more interesting to use its associated Strouhal number, since it usually remains in a narrow range for efficient flapping propulsion [1,62]. It is defined as

$$\mathrm{St} = \frac{A}{2\pi U}, \tag{22}$$

where A is the nondimensional beat amplitude, taken as the maximum peak-to-peak flapping foil amplitude. If the pivot axis is upstream the midchord ($a < 0$), the maximum amplitude is presumably reached at the trailing edge, whose z coordinate is $z_t(t) = z_s(1, t) = h(t) - (1 - a)\alpha(t) + (1 - a)^2 d(t)/2$, and $A = \overline{max(z_t) - min(z_t)}$.

Finally, for cruising, it is also widely used the cost of transport, instead of, or together with, the Froude efficiency, as a measure of the self-propulsion efficiency [63,64]. It is defined as the energy consumption per unit distance traveled by the vehicle. Although a dimensional form of this quantity is commonly used (e.g., with units of J/km), here we use a dimensionless version:

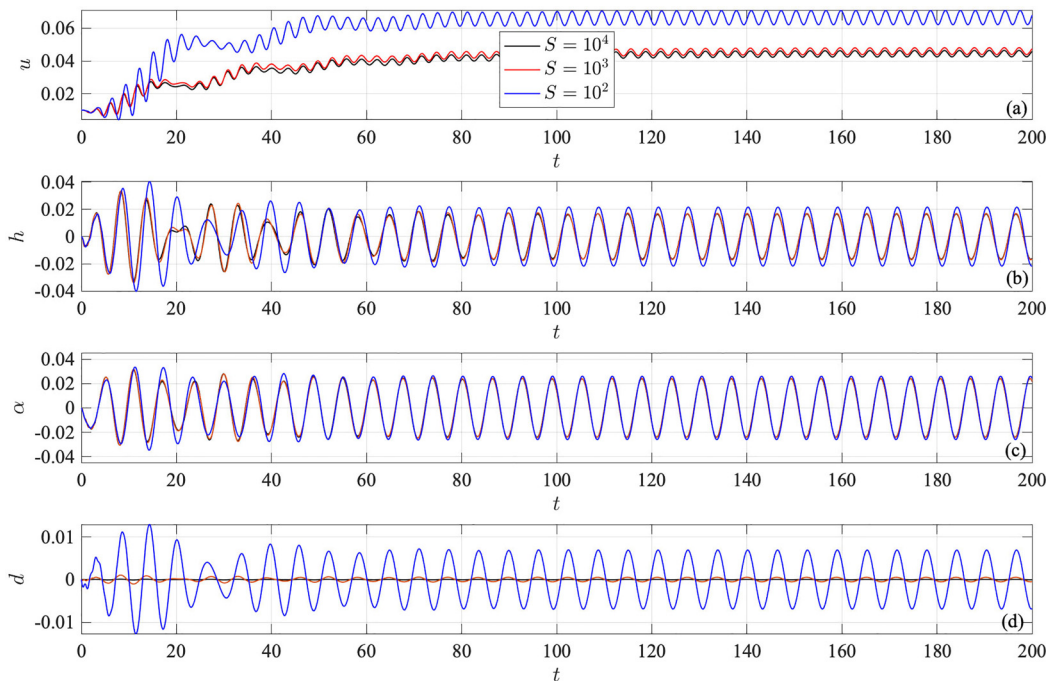$$CoT = \frac{\overline{\hat{C}_{P_i}}}{U}. \tag{23}$$

FIG. 2. Temporal evolutions of (a) the swimming velocity $u(t)$, (b) heaving $h(t)$, (c) pitching $\alpha(t)$, and (d) flexural deflection $d(t)$ motions for foil and vehicle mass ratios $R = 0.02$ and $R' = 0.2$, pivot axis and center of mass locations $a = -1$ and $x_0 = 0$, translational and torsional spring constants $k_h = 2.5$ and $k_\alpha = 3$, damper constants $b_h = b_\alpha = 0.05$, Lighthill number Li $= 0.1$, torque amplitude $\epsilon = 0.05$, and three values of the stiffness S indicated in (a).

III. SOLUTIONS AND DISCUSSION

A. Numerical solution

The system of ordinary differential equations (ODEs) (7) and (10)–(12) for $u(t)$, $h(t)$, $\alpha(t)$, and $d(t)$ is solved numerically using MATLAB's solver ode45 starting from vanishing initial conditions. Numerical solutions for decreasing values of the stiffness parameter S and typical values of the remaining nondimensional parameters (as discussed in Ref. [45] for a rigid foil) are shown in Fig. 2. In all cases, the solutions for all the variables consist of a transient phase much longer than the oscillating period, which eventually reach a permanent state with almost periodic oscillations around a constant mean. The mean is practically zero for h, α, and d, while $\bar{u} \to U > 0$ as discussed above. Notice that, for the selected set of values of the parameters, $h(t)$, $\alpha(t)$, and $d(t)$ remain small and, therefore, within the validity range of the model equations.

For very large S (10^4 and 10^3 in the figure) the foil behaves as a rigid foil, with d negligible and time evolutions of u, h, and α almost indistinguishable for $S = 10^3$ and $S = 10^4$. As S decreases to $S = 100$, $d(t)$ becomes noticeable and the swimming velocity U increases substantially, showing that, for the present set of values of the parameters, foil flexibility improves the propulsion performance in terms of swimming speed when all the rest of the vehicle and foil characteristics remain the same. Another feature of the solutions, which will be manifest in the perturbation analytical solution described in Sec. III B, is that, contrary to $u(t)$, both $h(t)$ and $\alpha(t)$ remain almost unaltered in the permanent state for $S = 100$ when $d(t)$ is no longer negligible. Thus, flexibility barely affects to the passive heaving and pitching motions of the foil but, nonetheless, it significantly affects its propulsive performance.

B. Asymptotic analytical solution

Although the numerical solution of the system of ODEs is straightforward, much insight about the propulsion performance may be gained by taking advantage of the small torque intensity ϵ and the large stiffness ratio S to obtain analytical approximate solutions for $h(t), \alpha(t), d(t)$, and $u(t)$ using perturbation methods. It will also be assumed that $u = 1/k \ll 1$, which constitutes an additional limitation of the asymptotic solution in relation to the numerical solution of the model equations for small ϵ and large S.

From the structure of the numerical solution described in the previous section, one may assume two time scales: a fast time t, associated to the period of the torque oscillations, and a slower time

$$\tau = B\epsilon^b t \tag{24}$$

associated to the transient towards the permanent oscillatory state with constant mean, where the constants B and b have to be determined from the scaling of the different terms in the equations. Since we are considering the small deflection approximation, we assume that $S \gg 1$. In the rigid-foil case ($S \to \infty, d = 0$), it was shown in Ref. [45] that $b = 4/3$ and the lowest-order solution can be written (discarding an irrelevant fast transient decay from the initial conditions) as

$$h(t, \tau) \sim \epsilon H_1 \sin(t + \phi_{h1}) + \dots, \quad \alpha(t, \tau) \sim \epsilon A_1 \sin(t + \phi_{a1}) + \dots, \tag{25}$$

$$u(t, \tau) \sim \epsilon^{4/3} u_1(\tau) + \epsilon^2 u_2(t) + \dots, \quad u_1(\tau) = U_1 w_1(\tau), \tag{26}$$

where functions $w_1(\tau)$ and $u_2(t)$, constants $H_1, A_1, \phi_{h1}, \phi_{a1}, U_1$, and the slow-time constant B, are all obtained analytically (see Appendix C). $w_1(\tau \to \infty) = 1$, so that the lowest-order swimming speed is $U \sim \epsilon^{4/3} U_1$. The scalings for h and α are easily derived from Eqs. (10)–(11) taking into account that $\hat{C}_{M_i} \sim \epsilon$ in the right-hand side of Eq. (11) and the asymptotic expansions of the remaining coefficients in the right-hand sides of Eqs. (10)–(11) when the large-k approximation of the different functions of k appearing in them are used (see Appendix D, where the formal general expansions of $\hat{C}_L, \hat{C}_T, \hat{C}_F$, and $\hat{C}_T$ in the present flexible case are given), whose first terms coincide with those for the rigid case when $S \gg 1$). The scaling for u and τ comes from the balance between drag and thrust in Eq. (7) using the expansions for u and $\hat{C}_T$.

When flexibility effects are taken into account, the new equation (12) with $S \gg 1$, together with the expansion for $\hat{C}_F$ (see Appendix D, where it is shown that the lowest order of $\hat{C}_F$ is also ϵ, like those of h and α) imply that

$$d \sim \epsilon S^{-1}, \tag{27}$$

so that d is much smaller than ϵ. Hence, this small deflection does not affect to h and α at their lowest orders because it is much smaller than ϵ, and the lowest-order solution (25) remains the same as that for a rigid foil (given in Appendix C; this feature was anticipated by the numerical solution described in Sec. III A). However, it may affect the swimming velocity u, which is smaller than ϵ at its lowest order. In fact, we will consider the deflection range where this does happen; i.e., the distinguished limit $S^{-1} \sim \epsilon^m$ such that flexibility $d \sim \epsilon^{1+m} = \epsilon^{m_1}$ modifies the swimming velocity at its lowest order. The value of m (or $m_1 = 1 + m$) can be derived taking into account the expansions of u and $\hat{C}_T$ [see Appendix D, where the power $n_1 = 4/3$, like in the first term of u in (26)]. Knowing that the first term in $\hat{C}_T$, or order ϵ^2, has zero mean and does not contributes to the mean swimming velocity, and balancing the second and third terms, which also match the drag term $\text{Li} \, u^2$, it results $1 + m_1 = 8/3$; i.e., $m_1 = 5/3$ and $m = 2/3$. Thus we define

$$S = \epsilon^{-2/3} S_1, \tag{28}$$

with S_1 of order unity, and the expansion

$$d(t, \tau) \sim \epsilon^{5/3} d_1(t, \tau) + \epsilon^{7/3} d_2(t, \tau) + \dots. \tag{29}$$

Substituting into Eq. (12) and using the expansion for $\hat{C}_F$ from Appendix D one gets, at the lowest order, $d_1(t)$ in terms of $h_1(t) = H_1 \sin(t + \phi_{h1})$ and $\alpha_1(t) = A_1 \sin(t + \phi_{a1})$,

$$d_1 = \frac{(a^2 + 1/4 + RI_a)H_1 \sin(t + \phi_{h1}) + [a(a^2 + 1/2) - RI_d]A_1 \sin(t + \phi_{a1})}{\frac{a^2 + 1/3}{3(1-a)^2} S_1}, \tag{30}$$

which can be written as

$$d_1 = D_1 \sin(t + \phi_{d1}), \tag{31}$$

with

$$D_1 = \sqrt{a_h^2 + a_a^2 + 2a_h a_a \cos(\phi_{h1} - \phi_{a1})}, \quad \phi_{d1} = \arctan \frac{a_h \sin \phi_{h1} + a_a \sin \phi_{a1}}{a_h \cos \phi_{h1} + a_a \cos \phi_{a1}}, \tag{32}$$

$$a_h = \frac{(a^2 + 1/4 + RI_a)H_1}{\frac{a^2 + 1/3}{3(1-a)^2} S_1}, \quad a_a = \frac{[a(a^2 + 1/2) - RI_d]A_1}{\frac{a^2 + 1/3}{3(1-a)^2} S_1}. \tag{33}$$

On the other hand, substituting (24)–(29) and the expansion of $\hat{C}_T$ given in Appendix D (with $b = n_1 = 4/3$, $n_2 = 2$, $n_3 = 8/3$) into Eq. (7), at the orders ϵ, ϵ^2, and $\epsilon^{8/3}$ we get, respectively, the following equations:

$$\frac{\partial u_1}{\partial t} = 0, \tag{34}$$

$$R' \frac{\partial u_2}{\partial t} = A_1 \{H_1 \cos(2t + \phi_{h1} + \phi_{a1}) + aA_1 \cos[2(t + \phi_{a1})]\}, \tag{35}$$

$$R'\left(\frac{\partial u_3}{\partial t} + B \frac{\partial u_1}{\partial \tau}\right) + Liu_1^2 = \left\{C_0 + H_1 A_2 \cos(2t + \phi_{h1} + \phi_{a2}) + A_1 H_2 \cos(2t + \phi_{a1} + \phi_{h2})\right.$$

$$+ 2aH_1 D_1 \cos(2t + \phi_{h1} + \phi_{d1}) - \frac{H_1 D_1}{2} \sin(2t + \phi_{h1} + \phi_{d1})$$

$$+ \left(5a^2 + \frac{3}{4} - A_{l2}\right)\frac{A_1 D_1}{2} \cos(2t + \phi_{a1} + \phi_{d1}) + \left(\frac{1}{2} - a\right)$$

$$\times \frac{A_1 D_1}{2} \sin(2t + \phi_{a1} + \phi_{d1}) + 2aA_1 A_2 \cos(2t + \phi_{a1} + \phi_{a2})\right\}$$

$$+ \frac{u^{1/2}}{\sqrt{\pi}} \left\{C + \frac{H_1^2}{2} \cos[2(t + \phi_{h1})] + \left(a - \frac{1}{2}\right)(a - 1)\frac{A_1^2}{2}\right.$$

$$\times \cos[2(t + \phi_{a1})] + \left(a - \frac{3}{4}\right) H_1 A_1 \cos(2t + \phi_{h1} + \phi_{a1})\right\}, \tag{36}$$

where

$$C_0 = \frac{1}{2}\left\{A_1 D_1\left[\left(a^2 + \frac{1}{4} + A_{l2}\right)\cos(\phi_{a1} - \phi_{d1}) + \left(a - \frac{1}{2}\right)\sin(\phi_{a1} - \phi_{d1})\right]\right.$$

$$- D_1 H_1 \sin(\phi_{d1} - \phi_{h1})\right\}, \tag{37}$$

$$C = \frac{H_1^2}{2} + \left(a - \frac{3}{4}\right)A_1 H_1 \cos(\phi_{h1} - \phi_{a1}) + \left(a - \frac{1}{2}\right)(a - 1)\frac{A_1^2}{2}. \tag{38}$$

Equations (34)–(35) coincide with those for the rigid-foil case (they do not depend on the lowest-order deflection d_1), resulting that u_1 only depends on τ, and yielding the same oscillatory function

$u_2(t)$ of the rigid-foil case (see Appendix C). On the other hand, Eq. (36) does depend on d_1. To avoid secular terms in the timescale t, we have the freedom within the two-scales perturbation method [34] to select the equation for $u_1(\tau)$ that cancels the nonoscillatory terms; i.e.,

$$R'B\frac{du_1}{d\tau} + \mathrm{Li}u_1^2 = C_0 + \frac{Cu_1^{1/2}}{\sqrt{\pi}}. \tag{39}$$

What remains of Eq. (36),

$$
\begin{aligned}
R'\frac{\partial u_3}{\partial t} = \Bigg\{ & H_1 A_2 \cos(2t + \phi_{h1} + \phi_{a2}) + A_1 H_2 \cos(2t + \phi_{a1} + \phi_{h2}) \\
& + 2a H_1 D_1 \cos(2t + \phi_{h1} + \phi_{d1}) - \frac{H_1 D_1}{2}\sin(2t + \phi_{h1} + \phi_{d1}) \\
& + \left(5a^2 + \frac{3}{4} - A_{l2}\right)\frac{A_1 D_1}{2}\cos(2t + \phi_{a1} + \phi_{d1}) + \left(\frac{1}{2} - a\right)\frac{A_1 D_1}{2}\sin(2t + \phi_{a1} + \phi_{d1}) \\
& + 2a A_1 A_2 \cos(2t + \phi_{a1} + \phi_{a2})\Bigg\} + \frac{u^{1/2}}{\sqrt{\pi}}\Bigg\{\frac{H_1^2}{2}\cos[2(t + \phi_{h1})] \\
& + \left(a - \frac{1}{2}\right)(a-1)\frac{A_1^2}{2}\cos[2(t + \phi_{a1})] + \left(a - \frac{3}{4}\right)H_1 A_1 \cos(2t + \phi_{h1} + \phi_{a1})\Bigg\},
\end{aligned} \tag{40}
$$

can easily be integrated to obtain explicitly u_3, except for an arbitrary function of τ. But with $u_1(\tau)$ and $u_2(t)$ would be enough since we are mostly interested in the lowest-order solution for u in terms of the slow time τ and the fast time t. Formally, the solution at the lowest order is (26), with the same $u_2(t)$ for a rigid foil given by Eq. (C5) in Appendix C, but with different function $u_1(\tau)$ and a different scaling constant B in the slow time τ.

To solve Eq. (39) it is convenient to rescale u_1 as in (26),

$$u_1(\tau) = U_1 w_1(\tau), \tag{41}$$

but now, according to (39), U_1 is given by the solution of the algebraic equation

$$\mathrm{Li}\, U_1^2 - \frac{C}{\sqrt{\pi}}U_1^{1/2} - C_0 = 0. \tag{42}$$

Selecting the slow-time scaling constant as

$$B = \frac{\mathrm{Li}U_1}{R'}, \tag{43}$$

which formally is the same of the rigid-foil case, but with a different swimming velocity U_1, Eq. (39) becomes

$$\frac{dw_1}{d\tau} = C^*\left(w_1^{1/2} - 1\right) + 1 - w_1^2, \qquad \text{with} \qquad C^* = \frac{C}{\sqrt{\pi}\mathrm{Li}\, U_1^{3/2}}. \tag{44}$$

In the rigid-foil case U_1 is such that $C^* = 1$ [see Eq. (C1) in Appendix C]. Equation (44) can be easily solved numerically with some initial condition [e.g., $w_1(0) = 0$]. The solution always satisfies $w_1(\infty) = 1$, so that the lowest-order nondimensional swimming velocity is $u \sim \epsilon^{4/3}U_1$. An explicit, analytical solution of Eq. (44) in the form $\tau = F(w_1; C^*)$ can be found, but the function F is so involved that it has no advantage whatsoever over the numerical solution. [For the rigid-foil case, with $C^* = 1$, F is much simpler, see (C3) in Appendix C.]

Contrary to the rigid-foil case, where U_1 is given explicitly, now one has to solve numerically the algebraic nonlinear equation (42). To that end it is convenient to start the iteration procedure from

the first correction to the rigid-foil value when $C_0 \to 0$. From (42),

$$U_1 \approx U_{1r}\left(1 + \frac{2\sqrt{\pi}C_0}{3CU_{1r}^{1/2}}\right), \quad C_0 \ll CU_{1r}^{1/2}, \tag{45}$$

where U_{1r} is the rigid-foil value of U_1 that makes $C^* = 1$. This seed to obtain U_1 will assure that one gets the correct physical solution of Eq. (42), that tends to the rigid-foil solution when $S \to \infty$. In addition to the mean swimming velocity $U \sim \epsilon^{4/3}U_1$ one can compute the other performance parameters defined in Sec. II B, which at their lowest order are given by

$$\overline{\widehat{C}_{P_i}} \sim \epsilon^2 A_1 \sin \phi_{a1}, \tag{46}$$

$$\eta \sim \epsilon^2 \frac{\text{Li}\, U_1^3}{A_1 \sin \phi_{a1}}, \tag{47}$$

$$CoT \sim \epsilon^{2/3} \frac{A_1 \sin \phi_{a1}}{U_1}, \tag{48}$$

$$St = \frac{A}{2\pi U} \sim \frac{\epsilon^{-1/3}}{\pi U_1}\left[H_1 + (1 + |a|)A_1 + \frac{1}{2}(1 + |a|)^2\epsilon^{2/3}D_1\right]. \tag{49}$$

Figure 3 compares the asymptotic lowest-order solutions for $u(t)$, $h(t)$, $\alpha(t)$, and $d(t)$ with the numerical solutions of the model equations for the same case plotted in Fig. 2 when $S = 1\,000$ and $S = 100$. The asymptotic solution captures quite well the numerical solution for large S, becoming poorer as the stiffness ratio S decreases to 100 or below, particularly for the swimming velocity $u(t)$. This is due to the limitation of the asymptotic solution to $u \ll \epsilon$, a constraint not shared by the model equations (remember that $\epsilon = 0.05$ in the figure). However, the agreement between both solutions remains excellent for $h(t)$, $\alpha(t)$, and $d(t)$ even for $S = 100$ (and below), notably for the pitch angle α.

The disagreement for the swimming velocity increases as one approaches the resonant values of the spring constants k_h and k_α, where the mean swimming velocity U reaches a pronounced maximum. Since h and α coincide with those for a rigid foil at the lowest order, so does the resonant value of the torsional spring constant $k_{\alpha r}$ for each value of the translational spring constant k_h [45]:

$$k_{\alpha r} = \frac{1}{2}\left[RI_a + a^2 + \frac{1}{8} + \frac{[a + R(a - x_0)]^2}{k_h - 1 - R}\right], \tag{50}$$

where the nondimensional moment of inertia $I_a = a^2 + 1/3$ (see Appendix B). Figure 4 compares the mean swimming velocity U obtained numerically from the model equations with the present lowest-order asymptotic solution as k_α is varied for the same values of the remaining parameters considered in Figs. 2 and 3, and for stiffnesses $S = 10^3$ and $S = 10^2$. Near the resonant value ($k_{\alpha r} \simeq 0.927$ in the present case, marked with a vertical dashed line in the figure) the asymptotic solution greatly overestimates the mean swimming velocity, even for large S. Also, for $S = 100$, the velocity prediction of the asymptotic is poor even for large k_α for the reason explained above in relation to Fig. 3. However, the lowest-order asymptotic solution yields correctly the scaling of U and, more importantly, predicts accurately the resonant values of the nondimensional parameters for optimal propulsion performance. Thus, the present asymptotic solution will guide the search for optimal propulsion performance given in the following section, but using the numerical solution of the model equations for quantitative results close to the resonance of the system.

C. Optimal propulsion performance

In this section we look for the best propulsion performance as described by the numerical solution of the model equations, and guided by the lowest-order asymptotic solution of Sec. III B. To that end we use a set of nondimensional parameters appropriate for a small aquatic vehicle (or a large
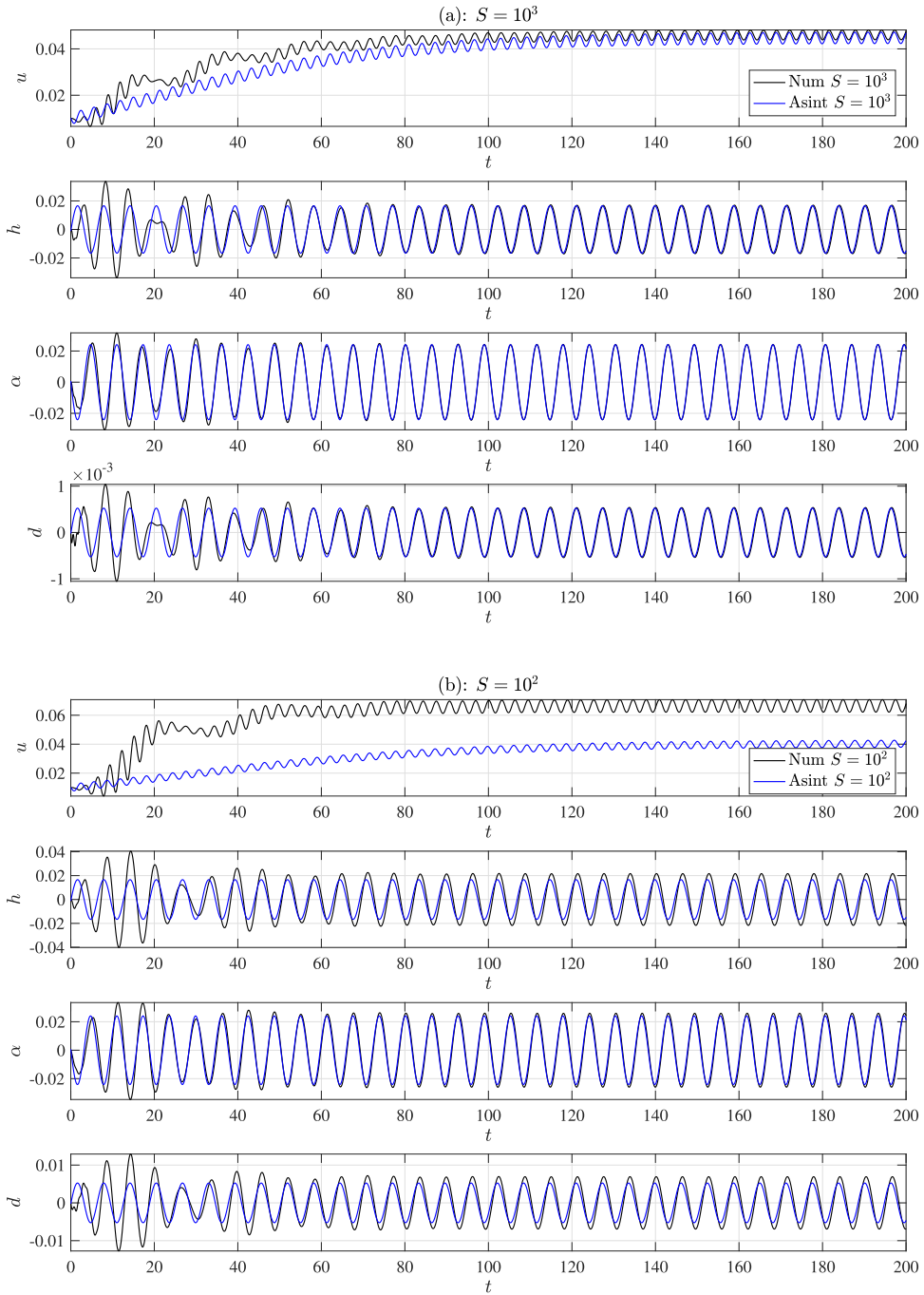
FIG. 3. Comparison between the lowest-order asymptotic solution (blue) and the numerical solution (black) for the same case plotted in Fig. 2 when (a) $S = 10^3$ and (b) $S = 10^2$. The quantities plotted vs time are the swimming velocity u, and the heaving (h), pitching (α), and flexural deflection (d) displacements.
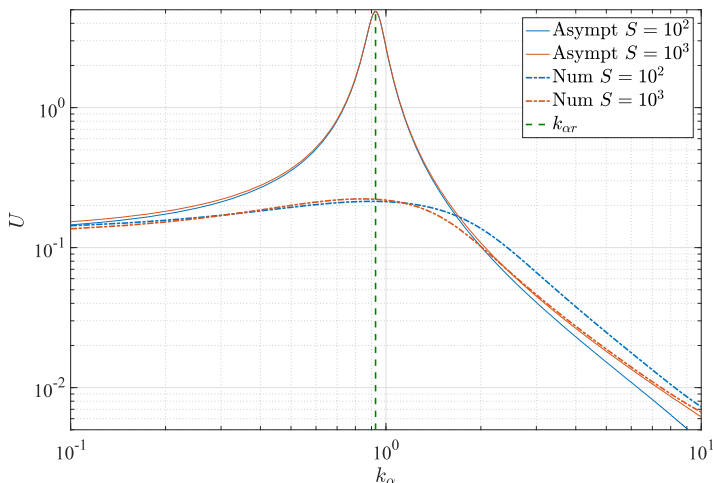
FIG. 4. Mean swimming velocity U vs torsional spring constant k_α for the same values of the remaining parameters used in Figs. 2 and 3, and for two values of the stiffness S, obtained from the lowest-order asymptotic solution (continuous lines) and from the numerical solution of the model equations (dashed-and-dotted lines). The vertical dashed line corresponds to the resonant value of k_α given by Eq. (50).

fish), varying mainly the stiffness parameter S, and also k_h, k_α, a, and Li. The fixed parameters are: $R = 0.02$, $R' = 0.2$, $x_0 = 0$, $b_h = b_\alpha = 0.05$, and $\epsilon = 0.05$. Note that although we select a small value of ϵ for the model assumptions to be valid, this does not restrict the analysis to a small actuating torque M_i, since it is scaled with the frequency ω and the foil chord length c [see Eq. (16)], being the actual torque also proportional to the span of the foil, so that it can be as large as desired by increasing the foil size and the actuating frequency, not being restricted to the propulsion of small aquatic vehicles.

According to the asymptotic results, the maxima of the swimming velocity are obtained for resonant values of k_α, $k_{\alpha r}(k_h, R, a, \dots)$, which at the lowest-order approximately coincide with the results for a rigid foil given by Eq. (50). Actually, it was shown in Ref. [45] that the maximum swimming velocity for a rigid foil was reached for large k_h. In that case, according to (50), $k_{\alpha r} \simeq (RI_a + a^2 + 1/8)/2$. Consequently, we select $k_h = 10$, large enough to reach the above asymptotic value of $k_{\alpha r}(k_h)$, and plot the performance parameters in Fig. 5 in the plane $k_\alpha - S$ for $Li = 0.1$ and $a = -1$; i.e., for the pivot axis at the leading edge, for which $k_{\alpha r} \simeq 0.634$, shown with vertical dashed lines in Fig. 5. We observe in Fig. 5(a) that the maximum swimming velocity (maximum thrust force) is reached close to this resonant value $k_{\alpha r}$ (at about $k_\alpha = 0.6$) and for a rigid foil; i.e., for $S \to \infty$. This result is in agreement with that previously found by Moore [53], who showed that torsional spring with a rigid foil is the optimal arrangement for thrust production in a fluid stream with fixed velocity. However, out of that resonance, for k_α larger than $k_{\alpha r}$, U increases as the stiffness S decreases, as already shown in the example of Fig. 2. Actually, the swimming velocities reach local maxima for lower values of S corresponding to the first resonant mode S_r associated to the stiffness of the foil. For instance, for $k_\alpha = 5$ we find a local maximum of $U \simeq 0.012$ for $S_r \approx 106$, which roughly coincides with the first resonant frequency associated to the stiffness of the foil with the present nondimensionalization [34,36]. In general, these local maxima of the swimming velocity are more than ten times smaller than the maxima of U for the first resonant mode associated to the torsional spring $k_\alpha = k_{\alpha r}$ when k_h is large. As found in previous models for an elastically mounted flexible foil in a fluid stream with fixed velocity, the resonances associated to the stiffness of the foil are eclipsed by the more efficient (from a thrust-producing point of view) resonance of the foil associated to its elastic support when the stiffness of the foil is high enough [26,53].
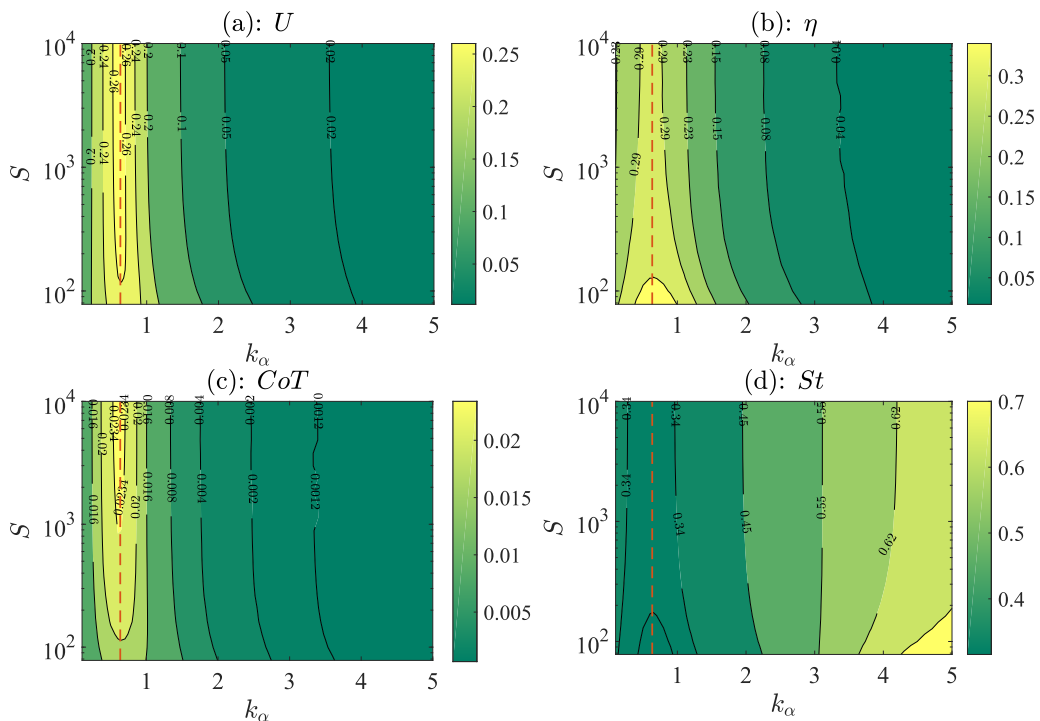
FIG. 5. Contours of (a) mean swimming velocity U, (b) propulsive efficiency η, (c) cost of transport CoT, and (d) Strouhal number St in the (k_α, S) plane for $R = 0.02$, $R' = 0.2$, $x_0 = 0$, $b_h = b_\alpha = 0.05$, $\epsilon = 0.05$, $a = -1$, $Li = 0.1$, and $k_h = 10$. The vertical dashed lines correspond to $k_{\alpha r}$ given by (50).

Although the highest U is reached for a rigid foil with k_α very close to $k_{\alpha r}$, it is observed in Fig. 5(c) that in the present self-propulsion problem this configuration is also that with the highest cost of transport CoT, and with a propulsive efficiency, which is not the maximum one [Fig. 5(b)]. The highest propulsive efficiency is also reached close to this resonant value of the torsional spring constant $k_{\alpha r}$, but for flexible foils with S below 100. In the figure, η at $k_\alpha \simeq k_{\alpha r}$ increases from about 29.7% for $S \to \infty$ to about 35.1% for $S \approx 75$. At this value of S the CoT is also significantly smaller than for a rigid foil (0.018 versus 0.024). It is remarkable that this optimal performance around the resonant value of k_α corresponds to an almost constant value of the Strouhal number, about 0.32, in accordance with the range where many swimming and flying animals in many scales optimally cruise propelled by flapping fins and wings [1,62], including also fishes swimming by undulating their bodies at high enough Reynolds numbers [65–68], quite different from the present oscillatory swimming mode (see Sec. IV below). With the present model, for $k_\alpha = k_{\alpha r}$, St in Fig. 5(d) ranges from 0.328 as $S \to \infty$, to 0.317 for $S \approx 75$.

Figure 6 shows the propulsive performance as one moves the pivot axis downstream of the foil ($a > -1$) maintaining the resonant value $k_{\alpha r}$ (actually, Fig. 6 is for $k_\alpha = 0.6$, where η is maximum for large S, very close to $k_{\alpha r}$). Figure 6(b) shows that the propulsive efficiency decreases, but remains practically unchanged for the optimal efficiency case just discussed (S below 100) if $-1 \leqslant a \lesssim -0.9$. However, the maximum swimming velocity, with the highest cost of transport, is reached for $a \approx -0.9$ for a rigid foil [Figs. 6(a) and 6(c)]. The Strouhal number remains practically unchanged for a near -1 [Fig. 6(d)].

We have seen that the maximum of U is reached close to the resonant value of k_α for a rigid foil. However, this behavior depends on the vehicle's drag through Li, as shown in Fig. 7, where contours of U divided by its rigid-foil counterpart U^{rigid} are plotted in the (m, S) plane. In the case
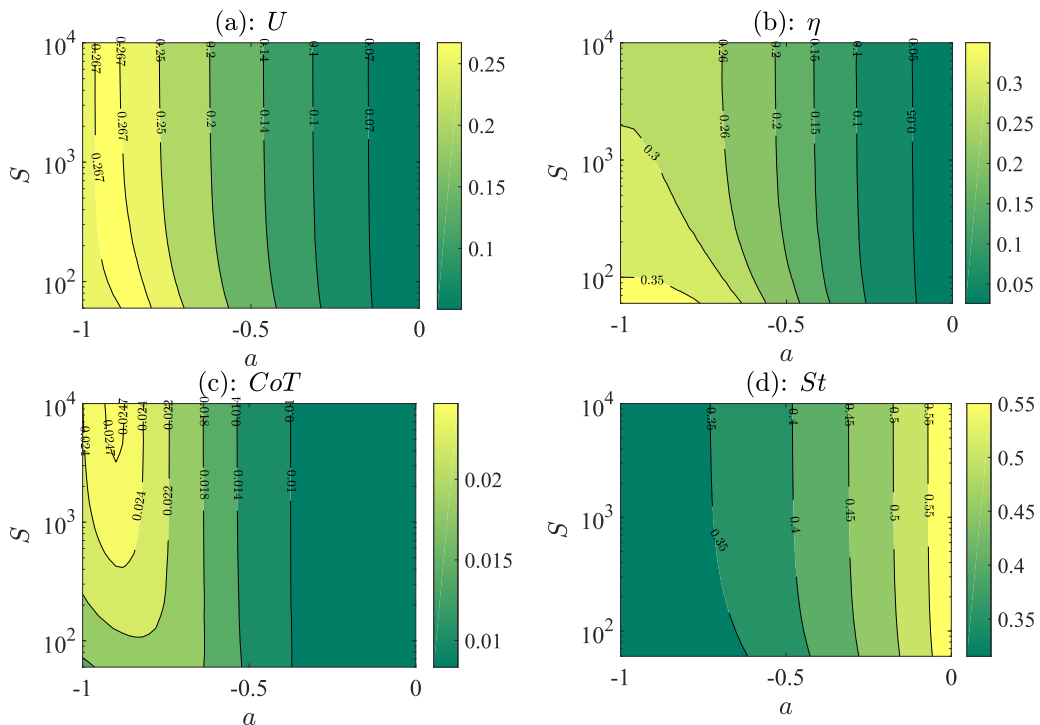
FIG. 6. Contours of (a) mean swimming velocity U, (b) propulsive efficiency η, (c) cost of transport CoT, and (d) Strouhal number St in the pivot-stiffness plane (a, S) for $R = 0.02$, $R' = 0.2$, $x_0 = 0$, $b_h = b_\alpha = 0.05$, $\epsilon = 0.05$, $Li = 0.1$, $k_h = 10$, and $k_\alpha = 0.6$.

with $Li = 0.1$ considered in Figs. 5 and 6, U/U^{rigid} decreases from unity as $S \to \infty$ to about 0.95 for $S \approx 75$. However, for $Li < Li^*(S)$, where the $Li^*(S)$ contour is marked with 0 in Fig. 7, the maximum of U at resonance increases slightly with the flexibility of the foil. Thus, for $Li = 0.005$, U/U^{rigid} increases from unity as $S \to \infty$ to about 1.04 for $S \approx 75$. To show this different behavior, Fig. 8 reproduces the results of Fig. 5 but for $Li = 0.01$. Now, the highest U is reached for a flexible flow [S below 10^2, see Fig. 8(a)], but still close to the resonant value $k_{\alpha r}$. For this Li, the highest efficiencies and CoT are also reached at these lower values of S when $k_\alpha \approx k_{\alpha r}$ [Figs. 8(b) and 8(c)]. However, the corresponding Strouhal numbers [Fig. 8(d)] are significantly lower than those found in natural swimmers, an indication that this value of the Lighthill number is too low and difficult to achieve in nature (see discussion in the next section).

IV. COMPARISON OF OPTIMAL EFFICIENCY RESULTS WITH FISH PROPULSION DATA

The expressions for the force components and moment from linearized potential flow theory, which are coupled with the Euler-Bernoulli beam equation in the present self-propulsion model, have been amply validated against numerical simulation and experimental data in the case of rigid foils [69–73], surprisingly showing a good agreement even for not so small amplitude of the oscillations, and for flexible foils [36,46,48]. The self-propulsion model with rigid foils has also been validated recently against high-fidelity numerical simulations for rigid foils [45,74]. However, to our knowledge, no numerical results about bodies self-propelled by flexible flapping foils elastically mounted are available to compare with. For that reason, to assess the validity of the model, we compare in Fig. 9 the results of the theory for the Strouhal number vs. the Lighthill number with experimental data for the swimming kinematics of several fishes compiled by Eloy [65], and with theoretical results derived by this author.
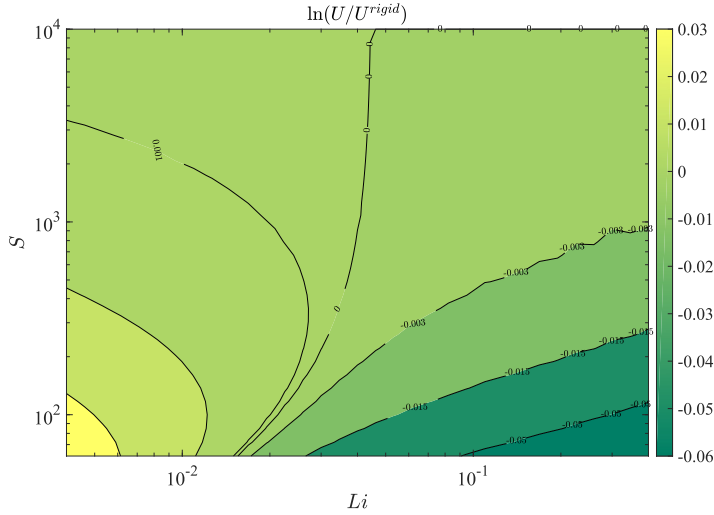
FIG. 7. Contours of $\ln(U/U^{\text{rigid}})$ in the (Li, S) plane for $R = 0.02$, $R' = 0.2$, $x_0 = 0$, $b_h = b_\alpha = 0.05$, $\epsilon = 0.05$, $a = -1$, $k_h = 10$, and $k_\alpha = 0.6$.

Actually, Eloy's theoretical results [65], based on Lighthill's elongated-body theory [75], are for undulatory swimming, qualitatively and quantitatively very different from the oscillatory swimming mode based on oscillatory foils considered in the present model [7,76]. Consequently, we include in Fig. 9 only the data for "scombrids" and "other fishes" compiled by Eloy [65], which include
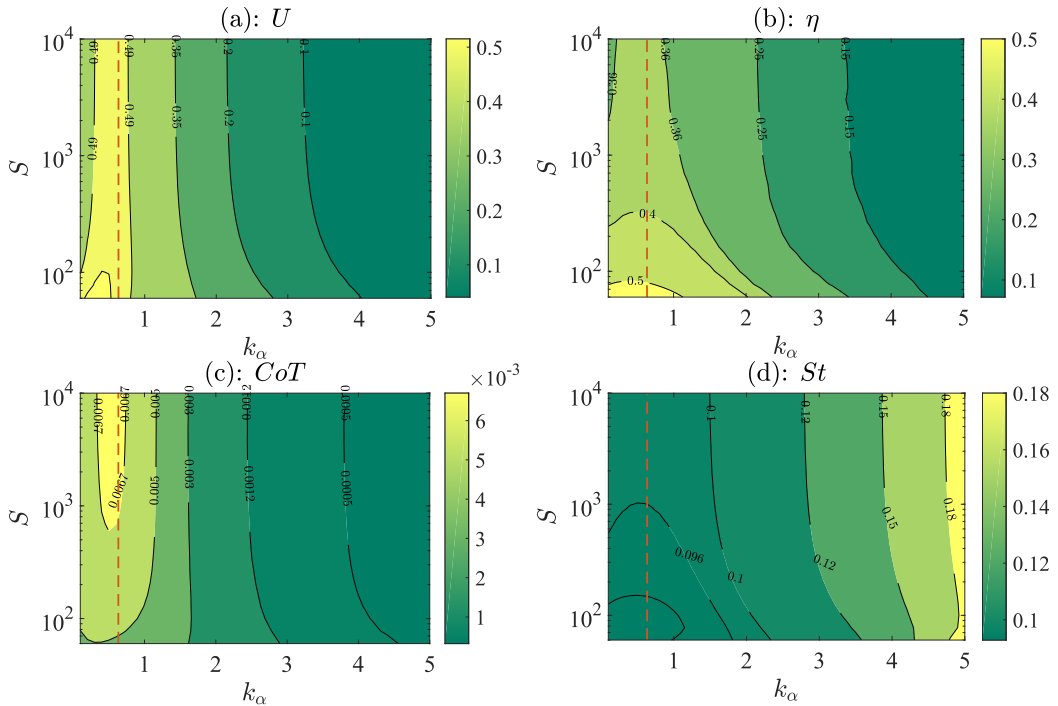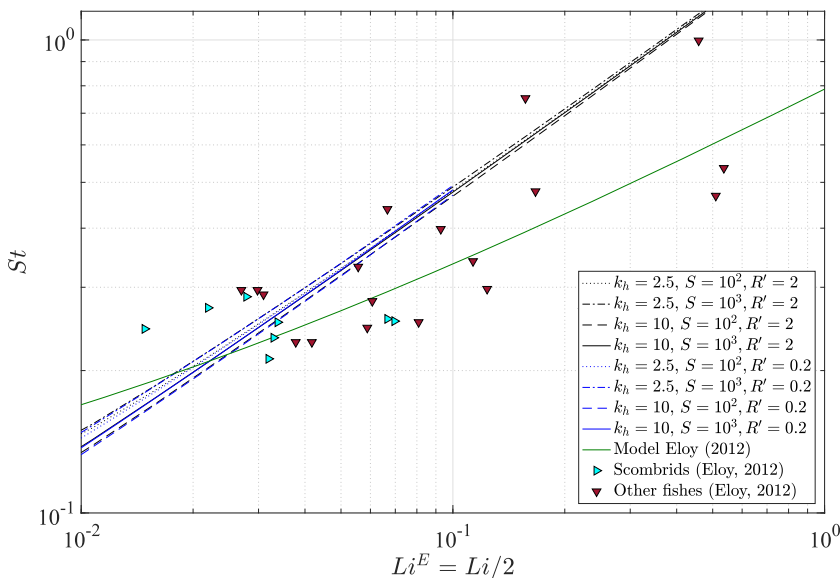

FIG. 8. As in Fig. 5, but for Li = 0.01.

FIG. 9. Strouhal number for maximum efficiency η as k_α is varied versus Lighthill number for several values of k_h, S, and R', as indicated in the legend. The green continuous line is Eloy's (2012) model for undulating swimming [65] and the symbols are experimental data for several fishes, both model and data taken from Fig. 4 in Ref. [65] (see main text for more details).

several species of mackerels, tunas, bonitos, daces, and goldfishes, among others. These fishes are mostly propelled by the thrust produced by their caudal fin oscillatory motion, being negligible the thrust contribution by the body motion [7,76]. Incidentally, tunas are among the fastest and most efficient swimming fishes in sustained cruise [77], and precisely they are endowed by nature with a long, almost rigid-fin tail, thus approximating better the assumptions of the present model. The other species considered in Fig. 9, though all of them are mostly propelled by their caudal fin oscillatory motion, have more flexible caudal fins. This fact, together with the variable contribution of the body undulatory motion to their propulsion, may explain part of the scattering in the experimental data. For the comparison in Fig. 9 we use the Lighthill number defined by Eloy, Li^E, which is related to that defined in Eq. (8) through $\mathrm{Li}^E = (\pi c/s)\mathrm{Li}$. Since the present theory is for two-dimensional foils, i.e., for large aspect ratio s/c, and it ranges from 4.5–10 in mackerels and tunas [78], for simplicity we have selected $s/c = 2\pi$, so that $\mathrm{Li}^E = \mathrm{Li}/2$. The Strouhal number defined in Eq. (22) is exactly the same used in Ref. [65].

We plot in Fig. 9 St resulting from the present model equations for translational spring constants $k_h = 2.5$ and 10, stiffness ratios $S = 10^3$ and 10^2, and vehicle's mass ratios $R' = 0.2$ and 2, corresponding, for each value of Li, to the highest efficiency η when k_α is varied, which approximately is reached at the rigid-foil resonant value $k_{\alpha r}$, as discussed above. The remaining parameters are fixed to $R = 0.02$, $x_0 = 0$, $b_h = b_\alpha = 0.05$, $\epsilon = 0.05$, and $a = -1$. The results are almost independent of R', particularly for $\mathrm{Li} \gtrsim 0.1$, in spite of the vehicle's mass disparity (note that, for $R = 0.02$, the value $R' = 0.2$ used in all previous figures roughly corresponds to a vehicle's mass ten times larger than that of its propeller, while $R' = 2$ corresponds to a vehicle about 100 times heavier than its propeller). Similar behavior is observed for the dependencies of St on k_h and S as Li is varied, in such a way that for $\mathrm{Li} \gtrsim 0.1$ the optimal Strouhal with the present oscillatory swimming model collapses to $St \approx 1.75(\mathrm{Li}^E)^{0.57} = 1.18\mathrm{Li}^{0.57}$. This should be compared with the power law obtained by Eloy from his undulatory swimming model, $St \approx 0.75(\mathrm{Li}^E)^{1/3}$, also shown in Fig. 9. The scattering of the experimental data makes it difficult to decide which fits better, but it seems that the present model works slightly better for the thunniform swimmers, which are the scombrids in
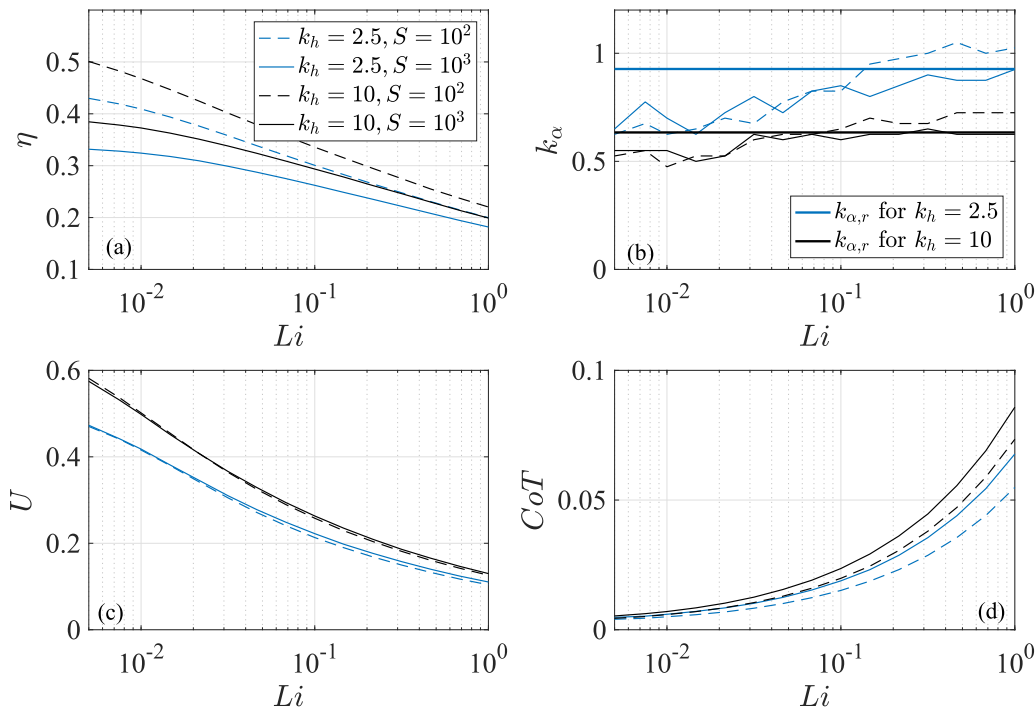
FIG. 10. (a) Optimal efficiencies η and (b) corresponding values of k_α, (c) U, and (d) CoT vs Li for the St-Li curves plotted in Fig. 9 when $R' = 2$. Also shown in (b) with thicker lines are the corresponding values of $k_{\alpha r}$ for each k_h.

Fig. 8 with lower Li, i.e., for typical swimmers where the primary mechanism for producing thrust is a prominent caudal fin.

Complementing Fig. 9, Fig. 10 shows the values of η, k_α, U, and CoT corresponding to the model curves plotted in Fig. 9 for $R' = 2$ (for $R' = 0.2$ the results practically coincide). The optimal efficiencies are reached for k_α close to $k_{\alpha r}$ [Fig. 10(b)], as discussed in Sec. III C, and obviously η increases as Li decreases, i.e., as the drag decreases. η may reach values higher than 50% when k_h is large (i.e., $k_h = 10$ in the figure) and $S = 100$, but for Li lower than about 0.01, too small to be achieved in nature as observed in Fig. 9. For all values of Li, the optimal η increases [Fig. 10(a)], and the corresponding CoT decreases [Fig. 10(c)], as the stiffness S decreases for a given k_h, as already discussed in Sec. III C. However, as it was also shown in that section, the swimming velocity U increases slightly with the stiffness S at these resonant values of k_α, except for very low, and unrealistic, values of Li [Fig. 10(c)].

V. CONCLUSION

A model for the locomotion of an aquatic vehicle self-propelled by a flexible foil elastically supported and actuated by an oscillatory torque is used to gain insight about the optimal propulsion conditions. Particularly, the conditions for which the flexibility of the foil enhances the propulsive and cruising performance. The model is based on linear potential flow theory coupled with the structural Euler-Bernoulli beam equation, valid for small amplitudes of the passive pitching, heaving, and flexural motions of the foil that propels a vehicle with constant drag coefficient and independent mass. The rigid-foil case has been previously validated with numerical simulations for high Reynolds number locomotion.

An analytical perturbation solution, additionally limited to very small nondimensional swimming velocities, guides the search for optimal propulsion solutions of the four ordinary differential equations resulting from the model as the nondimensional parameters governing the problem are varied, for a given actuating torque amplitude nondimensionalized with the actuating frequency, fluid density, and foil chord length. The main parameters are the stiffness and mass ratio of the foil, S and R, longitudinal and torsional springs constants, k_h and k_α, vehicle's mass ratio and Lighthill (drag) number, R' and Li, and center of mass and pivot axis locations, x_0 and a. It is found that the maxima of thrust and swimming velocity are achieved at, or very close to, a resonant combination of k_α and k_h given by a simple analytical expression in terms of R, a, and x_0 only, in the limit of a rigid foil ($S \to \infty$) for Lighthill numbers common in fishes, and when the foil is actuated at, or near, the leading edge ($a = -1$). More particularly, the maximum occurs when k_h is sufficiently large and the resonant $k_{\alpha r}$ for $a = -1$ depends only on R. These maxima of the swimming velocity U are associated to maxima of the cost of transport. However, the highest propulsive efficiencies, which are also reached for k_α close to $k_{\alpha r}$, increase as the stiffness S decreases, this being the main beneficial effect of the foil flexibility coupling with its elastic support on the propulsive performance according to the model. These results for optimal efficiency η are observed in the Lighthill number range of most fishes whose primary mechanism for producing thrust is a prominent oscillatory caudal fin, $0.02 \lesssim \text{Li} \lesssim 0.2$, almost independently of the remaining parameters, with a corresponding Strouhal number lying in a narrow range around 0.32, in agreement with many experimental data on the optimal cruise swimming of these fishes. As Li decreases, U and η increases and CoT decreases, reaching for Li ≈ 0.02 a propulsive efficiency close to 45%. Below this Li, the swimming velocity U may become slightly larger for a flexible foil than for its rigid counterpart, and the efficiency predicted by the model becomes larger than 50%, but so low values of Li are not reached even by the most efficient fishes in sustained cruise.

Summarizing, the following design guidelines follow from the present model results. First, and obviously, for optimal cruising performance one has to minimize the Lighthill number by reducing the vehicle's drag coefficient C_D as much as possible. Then one has to fix a sufficiently large (nondimensional) longitudinal spring constant k_h and a nondimensional torsional spring constant k_α close to its resonant value $k_{\alpha r}$, which for large k_h only depends on R and a. The pivot point location has to be selected close to the leading edge ($a \to -1$) for best performance, and R is selected from the foil geometry and density. From the relations between k_h and k_α and their dimensional counterparts, $k_h = 4\tilde{k}_h/(\pi \rho s c^2 \omega^2)$ and $k_\alpha = 8\tilde{k}_\alpha/(\pi \rho s c^4 \omega^2)$, and given the actuating torque, $M_i = \epsilon \pi \rho c^4 \omega^2/8$, one may select the actuating frequency ω and the foil size (i.e., c and s, with $s/c \gg 1$) for given values of $\tilde{k}_h$ and $\tilde{k}_\alpha$ and for any given $\epsilon \ll 1$. Alternatively, one may select ω, $\tilde{k}_h$, and $\tilde{k}_\alpha$ for given M_i, s, and c, or any other combination between these quantities. Finally, one may select the stiffness of the foil, actually the combination of Young's modulus and foil thickness $E\gamma^3$ entering in the dimensionless stiffness S, to achieve either maximum cruising speed or efficiency, or both. If Li $\gtrsim 0.02$, which will be the usual case because it would be rather difficult to get a smaller Li, maximum cruising speed U, but with high cost of transport, is achieved with a rigid foil ($S \gtrsim 10^3$, would be enough according to the present results), while maximum cruising efficiency η would be obtained for $S \lesssim 10^2$. An intermediate value of S can be fine tuned with the model for best global performance.

APPENDIX A: THRUST, LIFT, MOMENT, AND FLEXURAL COEFFICIENTS

The following expressions for the coefficients corresponding to the quartic foil's deflection (4) are taken from Refs. [36,46], written in the present notation and for nonconstant stream velocity

$u(t) = 1/k(t)$. Note that $v = \dot{h}$.

$$\hat{C}_T = -(\alpha + 2ad)C_L + \frac{d}{2}\left(\frac{\ddot{\alpha}}{2} + a\ddot{d} - u\dot{d}\right) + \frac{\dot{d}}{2}\left(\frac{\dot{\alpha}}{2} + a\dot{d} - ud\right)$$

$$+ (\dot{\alpha} + 2a\dot{d})\left\{v + a\dot{\alpha} + \left(a^2 + \frac{1}{4}\right)\dot{d} - u(\alpha + 2ad) + \Gamma_0\Re\left[\frac{i}{k}\mathcal{C}(k) + \left(\frac{1+ik}{k}\right)\frac{2}{\pi}\mathcal{C}_1(k)\right]\right\}$$

$$- [v + a\dot{\alpha} - u(\alpha + 2ad) + a^2\dot{d}]\Gamma_0\Re\left[\frac{2i}{\pi}\mathcal{C}_1(k)\right] - d\,\Gamma_0\Re\left[i\mathcal{C}_2(k) + 2\frac{1+ik}{k}\frac{2}{\pi}\mathcal{C}_1(k)\right]$$

$$+ \dot{d}\,\Gamma_0\Re\left[\left(\frac{2i}{k^2} - \frac{2+ik}{k}\right)\frac{2}{\pi}\mathcal{C}_1(k) - \frac{\mathcal{C}_2(k)}{k}\right], \tag{A1}$$

$$\hat{C}_L(t) = -\dot{v} - a\ddot{\alpha} + u\dot{\alpha} + \dot{u}\alpha + A_{l2}(a)\ddot{d} + A_{l1}(a)(u\dot{d} + \dot{u}d) + \Re[\mathcal{C}(k)]u\Gamma_0(t), \tag{A2}$$

$$\hat{C}_M(t) = \frac{1}{2}\left[a\dot{v} + \left(a^2 + \frac{1}{8}\right)\ddot{\alpha} + \left(\frac{1}{2} - a\right)u\dot{\alpha} - a\dot{u}\alpha + A_{m2}(a)\ddot{d} + A_{m1}(a)u\dot{d} + A_{m0}(a)u^2d\right]$$

$$- \frac{1}{2}\left(\frac{1}{2} + a\right)\Re[\mathcal{C}(k)]u\Gamma_0(t), \tag{A3}$$

$$\hat{C}_F(t) = -\left(a^2 + \frac{1}{4}\right)\dot{v} - a\left(a^2 + \frac{1}{2}\right)\ddot{\alpha} + a(a-1)u\dot{\alpha} + A_{f2}(a)\ddot{d} + A_{f1}(a)u\dot{d} + A_{f0}(a)u^2d$$

$$+ \left(\frac{1}{2} + a + a^2\right)\Re[\mathcal{C}(k)]u\Gamma_0(t), \tag{A4}$$

where $\Re$ means real part, and

$$\Gamma_0(t) = -2\left[v + \left(a - \tfrac{1}{2}\right)\dot{\alpha} - u\alpha + A_{g1}(a)\dot{d} + A_{g0}(a)ud\right]. \tag{A5}$$

The following functions of k and a are used:

$$\mathcal{C}(k) = \frac{H_1^{(2)}(k)}{iH_0^{(2)}(k) + H_1^{(2)}(k)} = \mathcal{F}(k) + i\mathcal{G}(k), \tag{A6}$$

$$\mathcal{C}_1(k) = \frac{\frac{1}{k}e^{-ik}}{iH_0^{(2)}(k) + H_1^{(2)}(k)}, \quad \mathcal{C}_2(k) = \frac{H_2^{(2)}(k)}{iH_0^{(2)} + H_1^{(2)}(k)}, \tag{A7}$$

where (A6) is Theodorsen's function [61], and $H_n^{(2)}(z) = J_n(z) - iY_n(z)$, $n = 0, 1$, Hankel's function of the second kind and order n, related to the Bessel functions of the first and second kind $J_n(z)$ and $Y_n(z)$ [79];

$$A_{l2} = -\frac{13 + 48a^2 - 64a^3 + 24a^4}{48(1-a)^2}, \quad A_{l1} = \frac{3 + 12a - 12a^2 + 4a^3}{6(1-a)^2}, \tag{A8}$$

$$A_{m2} = \frac{2 + 25a - 12a^2 + 52a^3 - 64a^4 + 24a^5}{48(1-a)^2}, \tag{A9}$$

$$A_{m1} = \frac{-9 + 12a - 72a^2 + 56a^3 - 16a^4}{24(1-a)^2}, \quad A_{m0} = -\frac{3}{4(1-a)^2}, \tag{A10}$$

$$A_{f2} = -\frac{35 + 32a + 392a^2 - 320a^3 + 496a^4 - 512a^5 + 192a^6}{384(1-a)^2}, \tag{A11}$$

$$A_{f1} = \frac{1 + 8a - 18a^2 + 48a^3 - 32a^4 + 8a^5}{12(1-a)^2}, \quad A_{f0} = \frac{7 + 18a}{12(1-a)^2}. \tag{A12}$$

$$A_{g1} = \frac{15 - 48a + 96a^2 - 80a^3 + 24a^4}{48(1-a)^2}, \quad A_{g0} = \frac{3 - 24a + 24a^2 - 8a^3}{12(1-a)^2}. \tag{A13}$$

For a rigid foil ($d = 0$), C_L and C_M are the classical expressions by Theodorsen [61], but corrected by Greenberg [80] to account for the temporal variation of the streamwise velocity u, while C_T coincides with the expression derived in Ref. [81].

APPENDIX B: COEFFICIENTS IN EQS. (10)–(12)

The following expressions for the nondimensional moment of inertia I_a, and the other coefficients related to the flexural deflection $d(t)$, are for constant foil density and thickness, so that $x_0 = 0$. More general expressions for any distribution $\rho_s(x)$ and $\gamma(x)$ can be found in Refs. [27,82].

$$J_a = \frac{1}{2}\left[a^2 - \frac{2}{3}a - \frac{1}{3} + \frac{16}{15(1-a)^2}\right] \tag{B1}$$

$$I_a = a^2 + \frac{1}{3}, \quad J_d = \frac{-12 - 93a + 60a^2 - 110a^3 + 120a^4 - 45a^5}{90(1-a)^2} \tag{B2}$$

$$I_d = -a(1 + a^2), \quad K_d = \frac{141 + 168a + 1281a^2 - 1120a^3 + 1015a^4 - 840a^5 + 315a^6}{630(1-a)^2}. \tag{B3}$$

APPENDIX C: ASYMPTOTIC SOLUTION FOR THE RIGID-FOIL CASE

From Ref. [45], the lowest-order asymptotic solution for the rigid-foil case can formally be written as (24)–(26), with

$$b = \frac{4}{3}, \quad B = \frac{Li\,U_1}{R'}, \quad U_1 = \left(\frac{C}{\sqrt{\pi}Li}\right)^{2/3}, \tag{C1}$$

$$C = \frac{H_1^2}{2} + \left(a - \frac{3}{4}\right)A_1 H_1 \cos(\phi_{h1} - \phi_{a1}) + \left(a - \frac{1}{2}\right)(a - 1)\frac{A_1^2}{2}, \tag{C2}$$

$w_1(\tau)$ given implicitly as

$$\tau = 2\frac{w_1^2 - w_1^{1/2}}{w_1^{3/2} - 1}F\left[1, 1/3; 4/3, w_1^{3/2}\right], \tag{C3}$$

where F is Gauss's hypergeometric function, and with $\mathcal{H}_1 \equiv H_1 e^{i\phi_{h1}}$ and $\mathcal{A}_1 \equiv A_1 e^{i\phi_{a1}}$ solution of the linear complex equations

$$\begin{pmatrix} -(R+1) + b_h i + k_h & -(a + R(a - x_0)) \\ a + R(a - x_0) & RI_a + a^2 + 1/8 - 2b_\alpha i - 2k_\alpha \end{pmatrix} \cdot \begin{pmatrix} \mathcal{H}_1 \\ \mathcal{A}_1 \end{pmatrix} = \begin{pmatrix} 0 \\ 2 \end{pmatrix}. \tag{C4}$$

Finally,

$$u_2(t) = \frac{A_1}{2R'}\{H_1 \sin(2t + \phi_{h1} + \phi_{a1}) + aA_1 \sin[2(t + \phi_{a1})]\}. \tag{C5}$$

APPENDIX D: ASYMPTOTIC EXPANSIONS OF THRUST, LIFT, MOMENT, AND FLEXURAL COEFFICIENTS

The formal general expansions of $\hat{C}_L$, $\hat{C}_T$, $\hat{C}_F$, and $\hat{C}_T$ are given below using

$$\tau = B\epsilon^b t, \quad \frac{d}{dt} = \frac{\partial}{\partial t} + B\epsilon^b \frac{\partial}{\partial \tau}, \quad \frac{d^2}{dt^2} = \frac{\partial^2}{\partial t^2} + 2B\epsilon^b \frac{\partial^2}{\partial t \partial \tau} + B^2 \epsilon^{2b} \frac{\partial^2}{\partial \tau^2}, \quad b \geqslant 1, \tag{D1}$$

and

$$h(t,\tau) \sim \epsilon h_1(t,\tau) + \epsilon^{m_1} h_2(t,\tau) + \epsilon^{m_2} h_3(t,\tau) + \ldots, \quad 1 > m_1 > m_2 > \ldots, \tag{D2}$$

$$\alpha(t,\tau) \sim \epsilon \alpha_1(t,\tau) + \epsilon^{m_1} \alpha_2(t,\tau) + \epsilon^{m_2} \alpha_3(t,\tau) + \ldots. \tag{D3}$$

$$d(t,\tau) \sim \epsilon^{m_1} d_1(t,\tau) + \epsilon^{m_2} d_2(t,\tau) + \epsilon^{m_3} d_3(t,\tau) + \ldots, \tag{D4}$$

$$u(t,\tau) \sim \epsilon^{n_1} u_1(t,\tau) + \epsilon^{n_2} u_2(t,\tau) + \epsilon^{n_3} u_3(t,\tau) + \ldots, \quad 1 > n_1 > n_2 > \ldots, \tag{D5}$$

together with the approximations for $k \gg 1$

$$\mathrm{Re}[C(k)] = \frac{1}{2} + O(k^{-2}), \quad \mathrm{Re}\left[\frac{i}{k}C(k) + \left(\frac{1+ik}{k}\right)\frac{2}{\pi}C_1(k)\right]$$

$$= \frac{1}{(4\pi k)^{1/2}} + O(k^{-3/2}), \quad \mathrm{Re}\left[\frac{2i}{\pi}C_1(k)\right]$$

$$= \frac{1}{(4\pi k)^{1/2}} + O(k^{-3/2}), \quad \mathrm{Re}\left[iC_2(k) + 2\left(\frac{1+ik}{k}\right)\frac{2}{\pi}C_1(k)\right]$$

$$= -\frac{1}{2} + O(k^{-1/2}), \quad \mathrm{Re}\left[\left(\frac{2i}{k^2} - \frac{2+ik}{k}\right)\frac{2}{\pi}C_1(k) - \frac{C_2(k)}{k}\right]$$

$$= \frac{1}{(4\pi k)^{1/2}} + O(k^{-3/2}). \tag{D6}$$

The expansions are

$$\hat{C}_L \sim -\epsilon\left(\frac{\partial^2 h_1}{\partial t^2} + a\frac{\partial^2 \alpha_1}{\partial t^2}\right) - \epsilon^{m_1}\left(\frac{\partial^2 h_2}{\partial t^2} + a\frac{\partial^2 \alpha_2}{\partial t^2} - A_{l2}\frac{\partial^2 d_1}{\partial t^2}\right)$$

$$- \epsilon^{m_2,b+1,1+n_1}\left(\frac{\partial^2 h_3}{\partial t^2} + a\frac{\partial^2 \alpha_3}{\partial t^2} - A_{l2}\frac{\partial^2 d_2}{\partial t^2} + 2B\frac{\partial^2 h_1}{\partial t \partial \tau} + a2B\frac{\partial^2 \alpha_1}{\partial t \partial \tau} - \left(\frac{3}{2} - a\right)u_1\frac{\partial \alpha_1}{\partial t}\right.$$

$$\left. - \alpha_1\frac{\partial u_1}{\partial t} + u_1\frac{\partial h_1}{\partial t}\right) + O(\epsilon^{m_3}, \epsilon^{b+m_1}, \epsilon^{m_1+n_1}), \tag{D7}$$

$$\hat{C}_M \sim \epsilon\left[a\frac{\partial^2 h_1}{\partial t^2} + \left(a^2 + \frac{1}{8}\right)\frac{\partial^2 \alpha_1}{\partial t^2}\right] + \epsilon^{m_1}\left[a\frac{\partial^2 h_2}{\partial t^2} + \left(a^2 + \frac{1}{8}\right)\frac{\partial^2 \alpha_2}{\partial t^2} + A_{m2}\frac{\partial^2 d_1}{\partial t^2}\right]$$

$$+ \epsilon^{m_2,b+1,1+n_1}\left[a\frac{\partial^2 h_3}{\partial t^2} + \left(a^2 + \frac{1}{8}\right)\frac{\partial^2 \alpha_3}{\partial t^2} + A_{m2}\frac{\partial^2 d_2}{\partial t^2} + a2B\frac{\partial^2 h_1}{\partial t \partial \tau} + \left(a^2 + \frac{1}{8}\right)2B\frac{\partial^2 \alpha_1}{\partial t \partial \tau}\right.$$

$$\left. + \left(\frac{1}{2} - a\right)^2 u_1\frac{\partial \alpha_1}{\partial t} - a\alpha_1\frac{\partial u_1}{\partial t} + \left(\frac{1}{2} + a\right)u_1\frac{\partial h_1}{\partial t}\right] + O(\epsilon^{m_3}, \epsilon^{b+m_1}, \epsilon^{m_1+n_1}), \tag{D8}$$

$$\hat{C}_F \sim -\epsilon\left[\left(a^2 + \frac{1}{4}\right)\frac{\partial^2 h_1}{\partial t^2} + a\left(a^2 + \frac{1}{2}\right)\frac{\partial^2 \alpha_1}{\partial t^2}\right]$$

$$- \epsilon^{m_1}\left[\left(a^2 + \frac{1}{4}\right)\frac{\partial^2 h_2}{\partial t^2} + a\left(a^2 + \frac{1}{2}\right)\frac{\partial^2 \alpha_2}{\partial t^2} - A_{f2}\frac{\partial^2 d_1}{\partial t^2}\right]$$

$$- \epsilon^{m_2,b+1,1+n_1}\left[\left(a^2 + \frac{1}{4}\right)\frac{\partial^2 h_3}{\partial t^2} + a\left(a^2 + \frac{1}{2}\right)\frac{\partial^2 \alpha_3}{\partial t^2} - A_{f2}\frac{\partial^2 d_2}{\partial t^2} + \left(a^2 + \frac{1}{4}\right)2B\frac{\partial^2 h_1}{\partial t \partial \tau}\right.$$

$$+ a\left(a^2 + \frac{1}{2}\right)2B\frac{\partial^2\alpha_1}{\partial t\,\partial\tau} + \left(a^3 - \frac{a^2}{2} + a - \frac{1}{4}\right)u_1\frac{\partial\alpha_1}{\partial t} + \left(\frac{1}{2} + a + a^2\right)u_1\frac{\partial h_1}{\partial t}\Bigg]$$

$$+ O(\epsilon^{m_3}, \epsilon^{b+m_1}, \epsilon^{m_1+n_1}), \tag{D9}$$

$$\hat{C}_T \sim \epsilon^2\left[\alpha_1\frac{\partial^2 h_1}{\partial t^2} + a\alpha_1\frac{\partial^2\alpha_1}{\partial t^2} + \frac{\partial h_1}{\partial t}\frac{\partial\alpha_1}{\partial t} + a\left(\frac{\partial\alpha_1}{\partial t}\right)^2\right]$$

$$+ \epsilon^{1+m_1}\left[\alpha_1\frac{\partial^2 h_2}{\partial t^2} + \alpha_2\frac{\partial^2 h_1}{\partial t^2} + 2ad_1\frac{\partial^2 h_1}{\partial t^2} + a\alpha_1\frac{\partial^2\alpha_2}{\partial t^2} + a\alpha_2\frac{\partial^2\alpha_1}{\partial t^2} + \left(2a^2 + \frac{1}{4}\right)d_1\frac{\partial^2\alpha_1}{\partial t^2}\right.$$

$$- A_{l2}\alpha_1\frac{\partial^2 d_1}{\partial t^2} + \frac{\partial h_2}{\partial t}\frac{\partial\alpha_1}{\partial t} + \frac{\partial h_1}{\partial t}\frac{\partial\alpha_2}{\partial t} + 2a\frac{\partial h_1}{\partial t}\frac{\partial d_1}{\partial t} - d_1\frac{\partial h_1}{\partial t} + 2a\frac{\partial\alpha_1}{\partial t}\frac{\partial\alpha_2}{\partial t}$$

$$+ \left(3a^2 + \frac{1}{2}\right)\frac{\partial\alpha_1}{\partial t}\frac{\partial d_1}{\partial t} + \left(\frac{1}{2} - a\right)d_1\frac{\partial\alpha_1}{\partial t}\Bigg]$$

$$+ \epsilon^{2+n_1/2}\frac{u^{1/2}}{\sqrt{\pi}}\left[\left(\frac{\partial h_1}{\partial t}\right)^2 + \left(2a - \frac{3}{2}\right)\frac{\partial h_1}{\partial t}\frac{\partial\alpha_1}{\partial t} + \left(a - \frac{1}{2}\right)(a - 1)\left(\frac{\partial\alpha_1}{\partial t}\right)^2\right] + \ldots \tag{D10}$$

[1] G. S. Triantafyllou, M. S. Triantafyllou, and M. A. Grosenbaugh, Optimal thrust development in oscillating foils with application to fish propulsion, J. Fluid Structures **7**, 205 (1993).

[2] I. Yamamoto, Y. Terada, T. Nagamatu, and Y. Imaizumi, Propulsion system with flexible/rigid oscillating fin, IEEE J. Oceanic Eng. **20**, 23 (1995).

[3] M. S. Triantafyllou, G. S. Triantafyllou, and D. K. P. Yue, Hydrodynamics of fishlike swimming, Annu. Rev. Fluid Mech. **32**, 33 (2000).

[4] K. V. Rozhdestvensky and V. A. Ryzov, Aerohydrodynamics of flapping-wing propulsors, Prog. Aero. Sci. **39**, 585 (2003).

[5] G. V. Lauder, Fish locomotion: Recent advances and new directions, Annu. Rev. Mar. Sci. **7**, 521 (2015).

[6] J. Zhu, C. White, D. K. Wainwright, V. Di Santo, G. V. Lauder, and H. Bart-Smith, Tuna robotics: A high-frequency experimental platform exploring the performance space of swimming fishes, Sci. Robot. **4**, eaax4615 (2019).

[7] A. J. Smits, Undulatory and oscillatory swimming, J. Fluid Mech. **874**, P1 (2019).

[8] X. Wu, X. Zhang, X. Tian, X. Li, and W. Lu, A review on fluid dynamics of flapping foils, Ocean Eng. **195**, 106712 (2020).

[9] J. Sánchez-Rodríguez, F. Celestini, C. Raufaste, and M. Argentina, Proprioceptive Mechanism for Bioinspired Fish Swimming, Phys. Rev. Lett. **126**, 234501 (2021).

[10] P. Prempraneerach, F. S. Hover, and M. S. Triantafyllou, The effect of chordwise flexibility on the thrust and efficiency of a flapping foil, in *Proceedings of the 13th International Symposium on Unmanned Untethered Submersible Technology*, UUST, Durham, NH (2003), https://web.mit.edu/towtank/www/papers/FlexibleFoil_Paper.pdf.

[11] M. S. Triantafyllou, A. H. Techet, and F. S. Hover, Review of experimental work in biomimetic foils, IEEE J. Oceanic Eng. **29**, 585 (2004).

[12] D. N. Beal, M. S. Hover, M. S. Triantafyllou, J. C. Liao, and G. V. Lauder, Passive propulsion in vortex wakes, J. Fluid Mech. **549**, 385 (2006).

[13] G. V. Lauder and P. G. A. Madden, Fish locomotion: Kinematics and hydrodynamics of flexible foil-like fins, Exp. Fluids **43**, 641 (2007).

[14] S. Heathcote and I. Gursul, Flexible flapping airfoil propulsion at low Reynolds numbers, AIAA J. **45**, 1066 (2007).

[15] C. K. Kang, H. Aono, C. E. S. Cesnik, and W. Shyy, Effects of flexibility on the aerodynamic performance of flapping wings, J. Fluid Mech. **689**, 32 (2011).

[16] C. Marais, B. Thiria, J. E. Wesfreid, and R. Godoy-Diana, Stabilizing effect of flexibility in the wake of a flapping foil, J. Fluid Mech. **710**, 659 (2012).

[17] D. J. Cleaver, I. Gursul, D. E. Calderon, and Z. Wang, Thrust enhancement due to flexible trailing-edge of plunging foils, J. Fluids Struct. **51**, 401 (2014).

[18] B. Monnier, A. M. Naguib, and M. M. Koochesfahani, Influence of structural flexibility on the wake vortex pattern of airfoils undergoing harmonic pitch oscillation, Exp. Fluids **56**, 80 (2015).

[19] M. Jimreeves David, R. N. Govardhan, and J. H. Arakeri, Thrust generation from pitching foils with flexible trailing edge flaps, J. Fluid Mech. **828**, 70 (2017).

[20] W. Liu, Q. Xiao, and F. Cheng, A bio-inspired study on tidal energy extraction with flexible flapping wings, Bioinspir. Biomim. **8**, 036011 (2013).

[21] T. Quang Le and J. Hwan Ko, Effect of hydrofoil flexibility on the power extraction of a flapping tidal generator via two- and three-dimensional flow simulations, Renew. Energy **80**, 275 (2015).

[22] J. Wu, C. Shu, N. Zhao, and F. B. Tian, Numerical study on the power extraction performance of a flapping foil with a flexible tail, Phys. Fluids **27**, 013602 (2015).

[23] W. Liu, Q. Xiao, and Q. Zhu, Passive flexibility effect on oscillating foil energy harvester, AIAA J. **54**, 1172 (2016).

[24] G. Jeanmonod and M. Olivier, Effects of chordwise flexibility on 2D flapping foils used as an energy extraction device, J. Fluids Struct. **70**, 327 (2017).

[25] B. Zhu, P. Xia, Y. Huang, and W. Zhang, Energy extraction properties of a flapping wing with an arc-deformable airfoil, J. Renewable Sustainable Energy **11**, 023302 (2019).

[26] R. Fernandez-Feria and J. Alaminos-Quesada, Propulsion and energy harvesting performances of a flexible thin airfoil undergoing forced heaving motion with passive pitching and deformation of small amplitude, J. Fluids Struct. **102**, 103255 (2021).

[27] R. Fernandez-Feria and J. Alaminos-Quesada, Energy harvesting and propulsion of pitching airfoils with passive heave and deformation, AIAA J. **60**, 783 (2022).

[28] T. Y. Wu, Swimming of a waving plate, J. Fluid Mech. **10**, 321 (1961).

[29] J. Katz and D. Weihs, Hydrodynamic propulsion by large amplitude oscillation of an aerofoil with chordwise flexibility, J. Fluid Mech. **88**, 485 (1978).

[30] S. Alben, Optimal flexibility of a flapping appendage in an inviscid fluid, J. Fluid Mech. **614**, 355 (2008).

[31] S. Michelin and S. G. Llewellyn Smith, Resonance and propulsion performance of a heaving flexible wing, Phys. Fluids **21**, 071902 (2009).

[32] S. Alben, C. Witt, T. V. Baker, E. Anderson, and G. V. Lauder, Dynamics of freely swimming flexible foils, Phys. Fluids **24**, 051901 (2012).

[33] D. B. Quinn, G. V. Lauder, and A. J. Smits, Scaling the propulsive performance of heaving flexible panels, J. Fluid Mech. **738**, 250 (2014).

[34] D. Floryan and C. W. Rowley, Clarifying the relationship between efficiency and resonance for flexible inertial swimmers, J. Fluid Mech. **853**, 271 (2018).

[35] D. Floryan and C. W. Rowley, Distributed flexibility in inertial swimmers, J. Fluid Mech. **888**, A24 (2020).

[36] R. Fernandez-Feria and J. Alaminos-Quesada, Analytical results for the propulsion performance of a flexible foil with prescribed pitching and heaving motions and passive small deflection, J. Fluid Mech. **910**, A43 (2021).

[37] B. Thiria and R. Godoy-Diana, How wing compliance drives the efficiency of self-propelled flapping flyers, Phys. Rev. E **82**, 015303(R) (2010).

[38] S. Ramananarivo, R. Godoy-Diana, and B. Thiria, Rather than resonance, flapping wings flyers may play on aerodynamics to improve performance, Proc. Natl. Acad. Sci. USA **108**, 5964 (2011).

[39] P. A. Dewey, B. M. Boschitsch, K. W. Moored, H. A. Stone, and A. J. Smits, Scaling laws for the thrust production of flexible pitching panels, J. Fluid Mech. **732**, 29 (2013).

[40] M. Olivier and G. Dumas, A parametric investigation of the propulsion of 2D chordwise-flexible flapping wings at low Reynolds number using numerical simulations, J. Fluids Struct. **63**, 210 (2016).

[41] M. Olivier and G. Dumas, Effects of mass and chordwise flexibility on 2D self-propelled flapping wings, J. Fluids Struct. **64**, 46 (2016).

[42] A. Goza, D. Floryan, and C. Rowley, Connections between resonance and nonlinearity in swimming performance of a flexible heaving plate, J. Fluid Mech. **888**, A30 (2020).

[43] J. D'Adamo, M. Collaud, R. Sosa, and R. Godoy-Diana, Wake and aeroelasticity of a flexible pitching foil, Bioinspir. Biomim. **17**, 045002 (2022).

[44] Y. Zhang, C. Zhou, and H. Luo, Effect of mass ratio on thrust production of an elastic panel pitching or heaving near resonance, J. Fluids Struct. **74**, 385 (2017).

[45] P. E. Lopez-Tello, R. Fernandez-Feria, and E. Sanmiguel-Rojas, Efficient self-propelled locomotion by an elastically supported rigid foil actuated by a torque, Appl. Math. Model. **116**, 236 (2023).

[46] J. Alaminos-Quesada and R. Fernandez-Feria, Propulsion of a foil undergoing a flapping undulatory motion from the impulse theory in the linear potential limit, J. Fluid Mech. **883**, A19 (2020).

[47] P. D. Yeh and A. Alexeev, Free swimming of an elastic plate plunging at low Reynolds number, Phys. Fluids **26**, 053604 (2014).

[48] E. Sanmiguel-Rojas and R. Fernandez-Feria, Propulsion enhancement of flexible plunging foils: Comparing linear theory predictions with high-fidelity CFD results, Ocean Eng. **235**, 109331 (2021).

[49] M. M. Murray and L. E. Howle, Spring stiffness influence on an oscillating propulsor, J. Fluids Struct. **17**, 915 (2003).

[50] M. N. J. Moore, Analytical results on the role of flexibility in flapping propulsion, J. Fluid Mech. **757**, 599 (2014).

[51] A. W. Mackowski and C. H. K. Williamson, Effect of pivot point location and passive heave on propulsion from a pitching airfoil, Phys. Rev. Fluids **2**, 013101 (2017).

[52] D. Asselin and C. H. K. Williamson, 'Addition of Passive dynamics to a heaving airfoil to improve performance' in the Report by C. H. K. Williamson 'Fluid-Structure Interactions Employing Cyber-Physical Fluid Dynamics', Technical Report AFRL-AFOSR-VA-TR-2019-0114, Air Force Research Laboratory, 2019.

[53] M. N. J. Moore, Torsional spring is the optimal flexibility arrangement for thrust production of a flapping wing, Phys. Fluids **27**, 091701 (2015).

[54] T. Van Buren, D. Floryan, N. Wei, and A. J. Smits, Flow speed has little impact on propulsive characteristics of oscillating foils, Phys. Rev. Fluids **3**, 013103 (2018).

[55] P. D. Yeh, Y. Li, and A. Alexeev, Efficient swimming using flexible fins with tapered thickness, Phys. Rev. Fluids **2**, 102101(R) (2017).

[56] R. N. Hua, L. Zhu, and X. Y. Lu, Locomotion of a flapping flexible plate, Phys. Fluids **25**, 121901 (2013).

[57] X. Zhu, G. He, and X. Zhang, Numerical study on hydrodynamic effect of flexibility in a self-propelled plunging foil, Comput. Fluids **97**, 1 (2014).

[58] A. P. Hoover, R. Cortez, E. D. Tytell, and L. J. Fauci, Swimming performance, resonance and shape evolution in heaving flexible panels, J. Fluid Mech. **847**, 386 (2018).

[59] E. Demirer, O. A. Oshinowo, and A. Alexeev, Efficient aquatic locomotion using elastic propulsors with hybrid actuation, J. Fluid Mech. **922**, A21 (2021).

[60] W. Wang, H. Huang, and X.-Y. Lu, Optimal chordwise stiffness distribution for self-propelled heaving flexible plates, Phys. Fluids **32**, 111905 (2020).

[61] T. Theodorsen, General theory of aerodynamic instability and the mechanism of flutter, Technical Report TR 496, NACA, 1935.

[62] G. K. Taylor, R. L. Nudds, and A. L. R. Thomas, Flying and swimming animals cruise at a Strouhal number tuned for high power efficiency, Nature (London) **425**, 707 (2003).

[63] G. Gabrielli and T. von Kármán, What price speed? Specific power required for propulsion of vehicles, Mech. Eng. **72**(10), 3 (1950).

[64] D. Paniccia, L. Padovani, G. Graziani, and R. Piva, The performance of a flapping foil for a self-propelled fishlike body, Sci. Rep. **11**, 22297 (2021).

[65] C. Eloy, Optimal Strouhal number for swimming animals, J. Fluids Struct. **30**, 205 (2012).

[66] M. Gazzola, M. Argentina, and L. Mahadevan, Scaling macroscopic aquatic locomotion, Nature Phys. **10**, 758 (2014).

[67] M. Saadat, F. E. Fish, A. G. Domel, V. Di Santo, G. V. Lauder, and H. Haj-Hariri, On the rules for aquatic locomotion, Phys. Rev. Fluids **2**, 083102 (2017).

[68] D. Gross, Y. Roux, C. Raufaste, and M. Argentina, Drag analysis with a self-propelled flexible swimmer, Phys. Rev. Fluids **6**, 053101 (2021).

[69] R. L. Halfman, Experimental aerodynamic derivatives of a sinusoidally oscillating airfoil in two-dimensional flow, Technical Report TR 1108, NACA, 1952.

[70] Y. S. Baik, L. P. Bernal, K. Granlund, and M. V. Ol, Unsteady force generation and vortex dynamics of pitching and plunging aerofoils, J. Fluid Mech. **709**, 37 (2012).

[71] R. Fernandez-Feria, Note on optimum propulsion of heaving and pitching airfoils from linear potential theory, J. Fluid Mech. **826**, 781 (2017).

[72] R. Fernandez-Feria and E. Sanmiguel-Rojas, Comparison of aerodynamic models for two-dimensional pitching foils with experimental data, Phys. Fluids **31**, 057104 (2019).

[73] J. Alaminos-Quesada, Limit of the two-dimensional linear potential theories on the propulsion of a flapping airfoil in forward flight in terms of the Reynolds and Strouhal number, Phys. Rev. Fluids **6**, 123101 (2021).

[74] R. Fernandez-Feria, E. Sanmiguel-Rojas, and P. E. Lopez-Tello, Numerical validation of simple non-stationary models for self-propelled pitching foils, Ocean Eng. **260**, 111973 (2022).

[75] M. J. Lighthill, Large-amplitude elongated-body theory of fish locomotion, Proc. R. Soc. Lond. B **179**, 125 (1971).

[76] M. J. Lighthill, Hydromechanics of aquatic animal propulsion, Annu. Rev. Fluid Mech. **1**, 413 (1969).

[77] P. W. Webb, Form and function in fish swimming, Sci. Am. **251**, 72 (1984).

[78] M. W. Westneat and S. A. Wainwright, Mechanical design for swimming: Muscle, tendon, and bone (chap. 7 in special issue Tuna: Physiology, Ecology, and Evolution), Fish Physiol. **19**, 271 (2001).

[79] F. W. J. Olver, D. W. Lozier, R. F. Boisvert, and C. W. Clark, editors, *NIST Handbook of Mathematical Functions* (Cambridge University Press, Cambridge, 2010).

[80] J. M. Greenberg, Airfoil in sinusoidal motion in a pulsating stream, Technical Report TR 1326, NACA, 1947.

[81] R. Fernandez-Feria, Linearized propulsion theory of flapping airfoils revisited, Phys. Rev. Fluids **1**, 084502 (2016).

[82] R. Fernandez-Feria, Flutter stability analysis of an elastically supported flexible foil. Application to the energy harvesting of a fully-passive flexible flapping-foil of small amplitude, J. Fluids Struct. **109**, 103454 (2022).